Atmos. Chem. Phys., 23, 12571–12588, 2023
https://doi.org/10.5194/acp-23-12571-2023

Atmospheric Chemistry and Physics
Open Access
EGU

Chemical composition-dependent hygroscopic behavior of individual ambient aerosol particles collected at a coastal site

Li Wu[1,2,★], Hyo-Jin Eom[1,3,★], Hanjin Yoo[1,4], Dhrubajyoti Gupta[1], Hye-Rin Cho[1], Pingqing Fu[2], and Chul-Un Ro[1,4]

[1]Department of Chemistry, Inha University, Incheon 22212, Republic of Korea
[2]Institute of Surface-Earth System Science, School of Earth System Science, Tianjin University, Tianjin 300072, China
[3]Air Quality Research Division, National Institute of Environmental Research, Incheon 22689, Republic of Korea
[4]Particle Pollution Management Center, Inha University, Incheon 21999, Republic of Korea
★These authors contributed equally to this work.

Correspondence: Chul-Un Ro (curo@inha.ac.kr)

Received: 8 April 2023 – Discussion started: 2 May 2023
Revised: 16 August 2023 – Accepted: 29 August 2023 – Published: 9 October 2023

Abstract. This study investigated the hygroscopic behavior of individual ambient aerosol particles collected at a coastal site of Jeju Island, South Korea. The size of the particles changes along with the phase transitions during humidification and dehydration processes, and the chemical compositions of the particles were determined by optical microscopy and scanning electron microscopy–energy dispersive X-ray spectroscopy (SEM-EDX), respectively. Of the 39 particles analyzed, 24 were aged sea spray aerosols (SSAs), with diverse mixing ratios of Cl^- and NO_3^-.

The ambient SSAs exhibited multiple deliquescence and efflorescence transitions that were dominantly influenced by NaCl, $NaNO_3$, $MgCl_2$, $Mg(NO_3)_2$, and organic species covering the surface of the aged SSAs. For Cl-rich SSAs with $X_{(Na,Mg)Cl} > 0.4$, although some particles showed very slow water uptake at low relative humidity levels (RH $\simeq$ 30 %), two major transitions were observed during the humidification process. The first was at RH $\simeq$ 63.8 %, regardless of their chemical compositions, which is the mutual deliquescence relative humidity (MDRH) level; and the second was at RH 67.5 % to 73.5 %, depending on their chemical compositions, which are the final deliquescence relative humidity (DRH) levels. During the dehydration process, the Cl-rich SSAs showed single-stage efflorescence at RH 33.0 % to 50.5 %, due to simultaneous heterogeneous crystallization of inorganic salts. For Cl-depleted SSAs with $X_{(Na,Mg)Cl} < 0.4$, two prompt deliquescence transitions were observed during the humidification process. The first was at MDRH 63.8 %, and the second was at RH 65.4 % to 72.9 %. The mutual deliquescence transition was more distinguishable for Cl-depleted SSAs. During the dehydration process, step-wise transitions were observed at efflorescence RH levels (ERH 24.6 % to 46.0 % and 17.9 % to 30.5 %), depending on their chemical compositions.

Additionally, aged mineral particles showed partial or complete phase changes with varying RH due to the presence of SSAs and/or NO_3^- species. In contrast, non-reacted mineral and Fe-rich particles maintained their size during the entire hygroscopic process. The mixture particles of organic and ammonium sulfate (AS) exhibited lower deliquescence and efflorescence RH levels compared to pure AS salt, highlighting the impact of organic species on the hygroscopic behavior of AS. These findings emphasize the complexity of atmospheric aerosols and the importance of considering their composition and mixing state when modeling their hygroscopic behavior and subsequent atmospheric impacts.

Published by Copernicus Publications on behalf of the European Geosciences Union.

1 Introduction

Atmospheric aerosols play a significant role in the global climate by directly scattering or absorbing incoming solar radiation and indirectly serving as cloud condensation nuclei (Haywood and Boucher, 2000; Pandis et al., 1995). The hygroscopicity of ambient aerosol particles, critically depending on their compositions, is of vital importance in understanding their properties, including their effects on aerodynamic performance, cloud droplet nucleation efficiency, optical properties, and heterogeneous chemical reactivity with atmospheric gas-phase species (Krueger et al., 2003; ten Brink, 1998; Wang and Martin, 2007; Wu et al., 2020). However, the study of their hygroscopic behavior is challenging because ambient aerosols typically exist as complex mixtures of several chemical species, even at the individual particle level, due to multiphase interactions (Krieger et al., 2012; Pöschl and Shiraiwa, 2015; Schiffer et al., 2018).

Sea spray aerosols (SSAs) are a significant component comprising 25 %–60 % of atmospheric particulate matter mass (Finlayson-Pitts and Pitts, 2000; Song et al., 2022). Understanding the hygroscopic properties of SSAs is essential for study on aerosol–cloud interactions and global climate (Schill et al., 2015; Zieger et al., 2017), which, however, is still defective, owing to their complex chemical compositions (Cochran et al., 2017; Meskhidze et al., 2013; Xu et al., 2020). Nascent SSAs are formed when bubbles burst at the sea surface, generating both submicron and supermicron SSAs from film and/or jet drops (Quinn et al., 2015; Wang et al., 2017). The primary inorganic constituents of nascent SSAs are Na^+, Cl^-, and Mg^{2+}, followed by SO_4^{2-}, Ca^{2+}, K^+, and other minor compositions (Seinfeld and Pandis, 2006). Submicron nascent SSAs contain more organic species and fewer inorganic salts than supermicron ones (Ault et al., 2013; Prather et al., 2013; Wang et al., 2015). In pristine marine environments, the organics in SSAs mostly originate from phytoplankton activities in the sea, while in polluted marine environments, nonbiodegradable surfactants from anthropogenic waste runoff to the sea are supposed to be added (Cochran et al., 2016; Forestieri et al., 2016). Reactions of SSAs with various atmospheric species, such as NO_x/HNO_3, SO_2/H_2SO_4, and CH_3SO_3H, within minutes to hours of residence in air, further increase the complexity of the chemical compositions (Liu et al., 2007; Saul et al., 2006; ten Brink, 1998), leading to partially or fully reacted (or aged) SSAs after Cl depletion (Ault et al., 2014; Gard et al., 1998; Laskin et al., 2012; Pósfai et al., 1995; Wu et al., 2020). The further reactive uptake of N_2O_5 was also reported to be dependent on the chloride to nitrate ratio of the reacted SSAs and their phases (Ryder et al., 2014). In addition, SSAs interact with volatile organic carbons (VOCs) and secondary organic aerosols (SOAs) in the marine boundary layer (Su et al., 2022). The presence of primary and secondary organics, biogenic species, sea salt sulfates (ss-SO_4^{2-}), and nonsea-salt sulfates (nss-SO_4^{2-}) adds greater complexity to the interdependence of hygroscopic behavior and heterogeneous reactions in ambient SSAs (Ault et al., 2013; Beardsley et al., 2013; Keene et al., 2007; O'Dowd and de Leeuw, 2007; Prather et al., 2013).

Many studies have investigated the hygroscopic behavior of both airborne and laboratory-generated SSAs. It is generally accepted that sea-salt-containing particles result in higher hygroscopic factors in supermicron particles (Atkinson et al., 2015; Herich et al., 2009). Some single-particle measurements have been reported on ambient fine- and coarse-mode SSAs that are dominated by inorganic salt species. For example, environmental transmission electron microscopy was used to measure the deliquescence and efflorescence relative humidities (DRHs and ERHs) of NaCl-bearing aerosols, sulfate or chloride containing SSAs, and Mg-rich particles collected from clean and polluted environments (Semeniuk et al., 2007; Wise et al., 2007). It was found that NaCl moiety in sulfate- or chloride-containing SSAs underwent deliquescence at ~ 75 % RH, with the sulfate-bearing phases remaining insoluble, which is similar to the DRH of pure NaCl aerosols, whereas the DRH of the NaCl moiety was lowered in the presence of soluble compositions like $NaNO_3$. In a follow-up study, the DRHs and ERHs of laboratory-generated and ambient SSA particles were found to be consistent (Wise et al., 2009). Similar observations for marine aerosols with insoluble sulfate moieties and a highly hygroscopic NaCl moiety were also reported (Freney et al., 2010). In situ Raman spectrometry was used to probe the phase transitions of SSA droplets (80–100 µm) nebulized from seawater, which revealed that $CaSO_4 \cdot 0.5H_2O$ solidified at RH > 90 %, followed by the crystallization of NaCl and $KMgCl_3 \cdot 6H_2O$ at RH $\simeq 55$ % and ~ 44 %, respectively (Xiao et al., 2008). Optical microscopy combined with low Z particle energy-dispersive electron probe X-ray microanalysis (low Z particle EPMA) was used to determine 2-D growth factors, phase transition RHs, and chemical compositions in ambient aerosols, including nascent and reacted/aged SSAs (Ahn et al., 2010). However, the relationship between hygroscopic properties and the evolving chemical compositions and mixing states of ambient SSAs remains unclear.

Laboratory-generated inorganic salt particles have been utilized as surrogates to understand and parameterize the complex hygroscopic properties of SSAs for climate models. Since NaCl constitutes approximately 80 % of nascent SSAs by mass, the hygroscopic behavior of pure NaCl particles has been extensively studied for parameterizing the thermodynamic and optical properties and cloud activation efficiency of ambient SSAs (Niedermeier et al., 2008; Tang et al., 1997). However, the hygroscopic growth factors of ambient or laboratory-generated SSAs are reported to be differ-

ent from those of pure NaCl, possibly due to the presence of hydrates such as $MgCl_2 \cdot 6H_2O$, organic substances, or other impurities (Ahn et al., 2010; Guo et al., 2019; Kong et al., 2018; Rosati et al., 2021; Schindelholz et al., 2014; Zieger et al., 2017). Consequently, the hygroscopic properties of multicomponent systems such as mixed cation chlorides (Chan et al., 2000; Ge et al., 1996, 1998; Gupta et al., 2015a; Li et al., 2014), sodium salts of mixed anions (Chan et al., 1997; Chang and Lee, 2002; Freney et al., 2010; Gupta et al., 2015b), and other mixture systems such as NaCl–$MgSO_4$ (Woods et al., 2010), NaCl–$CaSO_4$ (Freney et al., 2010), and NaCl–$(NH_4)_2SO_4$ (Tobon et al., 2021) are of special relevance, which can serve as surrogates for ambient or reacted SSAs.

As discussed in detail elsewhere (Gupta et al., 2015a; Li et al., 2014), thermodynamic principles predict stepwise phase transitions in two-component inorganic solid salt mixtures, such as NaCl–KCl, NaCl–$MgCl_2$, and NaCl–$NaNO_3$, that can dissolve during the humidification process (Wexler and Seinfeld, 1991). When the mixing ratio of the two-component element is at a certain value, e.g., $X_{NaCl} = 0.38$ (or $X_{NaNO_3} = 0.62$) in the NaCl–$NaNO_3$ mixture, particles act like a single salt and exhibit a single-phase transition at its mutual DRH (MDRH), where the mixture is considered to have a eutonic composition. For particles with other mixing ratios, the first transition generally occurs at their MDRH, regardless of the specific ratios, and the resulting aqueous phase from partial deliquescence also possesses the eutonic composition. As RH further increases, partially dissolved particles continue to absorb water until the remaining solid component fully dissolves at the respective DRH, which is dependent on the salt moiety being richer in concentration. During the dehydration process, as RH decreases, the concentration of the richer salt moiety becomes more concentrated, leading to crystallization at their respective ERH level. The aqueous phase of the eutonic composition then effloresces at their mutual ERH (MERH) level as the RH further decreases.

Thermodynamic models, such as the Extended Aerosol Inorganics Model (E-AIM; http://www.aim.env.uea.ac.uk/aim/aim.php, last access: 18 March 2023; Ansari and Pandis, 1999; Carslaw et al., 1995; Clegg et al., 1998b, a; Wexler and Clegg, 2002) and the Aerosol Inorganic–Organic Mixtures Functional groups Activity Coefficients (AIOMFAC; http://www.aiomfac.caltech.edu/, last access: 18 March 2023; Zuend et al., 2008, 2011), can predict MDRHs and DRHs for multicomponent mixture systems. The DRH represents the solubility limit (saturation concentration) of a compound in a solution, defining a solid–liquid equilibrium. When a solid compound coexists with a saturated liquid mixture, it has a specific molar ion activity product (IAP) in that solution. The AIOMFAC model calculates IAP as a function of RH using ion activity coefficients, which remains constant, regardless of other mixture components. The corresponding RH becomes the DRH when the calculated IAP matches that of the saturated solutions. However, as efflorescence is a kinetic or rate-driven process, no general theoretical model can predict the efflorescence of single or multicomponent aerosol particles, and thus, the best way is through experimental observation (Cohen et al., 1987; Martin et al., 2000). Previous modeling and field studies have attributed the reduction in the hygroscopic growth of SSAs to the organic fractions (Ming and Russell, 2001; Vaishya et al., 2013; Zhang et al., 2014), whereas recent measurements suggest that organic species have an insignificant influence (Nguyen et al., 2017). Therefore, establishing a systematic correlation between the chemical compositions and hygroscopic behavior of ambient SSAs vis-à-vis the multicomponent inorganic surrogates is a priority with respect to understanding the hygroscopic properties of ambient SSAs and parameterizing phase changes for model applications.

Mineral particles, such as aluminosilicates and calcium carbonate, which are typically non-hygroscopic, can become hygroscopic when they are internally mixed with SSAs or react with gaseous species such as NO_x, SO_2, and organic acids in the presence of water vapor (Li et al., 2014; Tang et al., 2016). In fact, mineral dust and aged SSAs may exist as internal and/or external mixtures in the atmosphere (Geng et al., 2014). For instance, a Mg silicate particle coagulated with SSA partially increased in size only at the SSA region with increasing RH and was covered with an aqueous droplet caused by the complete dissolution of the SSA part in high RH (Semeniuk et al., 2007). Additionally, aluminosilicates coated with sulfur-bearing materials or internally mixed with sea salt particles can absorb water, although the aluminosilicates remained as solid phases (Freney et al., 2010).

In this study, we systematically investigated the hygroscopic behavior of ambient aerosols collected on Jeju Island, South Korea, together with their chemical compositions in various mixing states on a single-particle basis. In particular, the hygroscopic properties and chemical compositions of ambient SSAs were examined and compared with multicomponent inorganic surrogate systems containing Na^+, Mg^{2+}, Cl^-, and NO_3^-. The phase transitions were observed by monitoring the 2-D size changes in the particles as a function of RH under optical microscopy, and the hygroscopic curves and phase diagrams were derived. To determine the chemical compositions of the individual ambient aerosols and the spatial distribution of elements in the effloresced particles, we used scanning electron microscopy–energy dispersive X-ray spectroscopy (SEM-EDX) and analyzed their X-ray spectra and maps, respectively. Although ambient aerosols are complex in their compositions and hygroscopic properties, the detailed elucidation of their hygroscopic behavior according to chemical compositions of ambient aerosols can contribute to the ongoing efforts to improve our understanding of atmospheric aerosols and their impacts on global climate.

Figure 1. Location of the Gosan sampling site on Jeju Island, South Korea (map copyright: © Google Earth).

2 Experimental section

2.1 Samples

2.1.1 Ambient aerosol particles

Aerosol samples were collected on 16 and 17 April 2012 at the Gosan meteorological site (33.29° N, 126.16° E), which is located on the west coast of Jeju Island, South Korea (see Fig. 1). Ambient aerosols were loaded on transmission electron microscopy (TEM) grids (200 mesh Cu coated with Formvar stabilized with carbon; Ted Pella, Inc.) mounted on stages 2 and 3 of a three-stage cascade PM_{10} impactor (Dekati Ltd.) with aerodynamic cutoff diameters of 10–2.5 and 2.5–1.0 µm, respectively, at a flow rate of 10 L min^{-1}. Sampling durations for each stage were adjusted to collect an appropriate number of particles without overloading. The samples were put into black plastic boxes and sealed with Parafilm immediately after collection. These sealed samples were then stored in a refrigerator before the measurements. Stage 2 particles, which were sized between 10 and 2.5 µm, were used to measure the chemical composition and hygroscopic behavior in this study.

2.1.2 Laboratory-generated (Na, Mg)(Cl, NO_3) mixture particles

In previous studies (Gupta et al., 2015a, b; Zhang et al., 2004), aerosols of NaCl, $NaNO_3$, $Mg(NO_3)_2$, NaCl–$NaNO_3$, and NaCl–$MgCl_2$ were extensively investigated. As Na^+, Mg^{2+}, Cl^-, and NO_3^- are major species of the ambient SSAs collected in our samples, based on low Z particle EPMA results, we measured the hygroscopic behavior of a NaCl–$MgCl_2$–$NaNO_3$–$Mg(NO_3)_2$ surrogate system in this work to simulate ambient SSAs that contain similar major elements. Pure solutions (1.0 M each) of NaCl (> 99.9 % purity; Sigma-Aldrich), $MgCl_2 \cdot 6H_2O$, and $NaNO_3$ (99.9 % purity; Sigma-Aldrich) were prepared using de-ionized water (18 MΩ; Millipore Direct-Q®). The pure solutions were then mixed to obtain solutions with $[Cl^-] : [NO_3^-] = 3 : 1$, $1 : 1$, and $1 : 3$ (i.e., $X_{(Na,Mg)Cl} = 0.75$, 0.5, and 0.25), while maintaining the seawater ratio of $[Na^+] : [Mg^{2+}] = 9 : 1$ (Haynes, 2015), as the elemental ratio of Na and Mg in the ambient SSAs from our samples is also approximately 9. A single jet atomizer (HCT4810) was used to generate aerosol particles from the mixture solutions on hydrophobic TEM grids. Herein, a notation system is used to represent aerosol particles of NaCl–$MgCl_2$–$NaNO_3$–$Mg(NO_3)_2$ as (Na, Mg)(Cl, NO_3).

2.2 Hygroscopic property measurements

The experimental setup for measuring hygroscopic behavior consists of the following three main components: (a) a see-through impactor, (b) an optical microscope, and (c) a humidity control system. The TEM grid with aerosol particles was attached to the impaction plate in the see-through impactor, and the RH was controlled by mixing dry and wet gaseous N_2 (99.999 % purity) flows that were adjusted to obtain the desired RH in the range of ∼ 5.0 %–92.0 %. The humidity control system used wet N_2 gas obtained by bubbling through deionized water reservoirs. The RH was monitored by a digital hygrometer (testo 645) that was calibrated using a dew point hygrometer (M2-plus RH; GE) to provide RH readings with ±0.5 % reproducibility. A detailed discussion of the impactor and humidity-controlling system can be found elsewhere (Li et al., 2021). The particles were continuously imaged in RH 1 % steps, using a digital camera (Canon EOS 5D, with a full-frame Canon EF f/3.5 L macro USM lens) mounted on an optical microscope (Olympus BX51M) during the humidification process (by increasing RH from ∼ 5.0 % to 92.0 %), followed by the dehydration process (by decreasing RH from ∼ 92.0 % to 5.0 %). The changes in particle size with the variation in the RH were monitored by measuring the particle areas in the optical images to generate hygroscopic curves. Each humidity condition was sustained for at least 2 min to allow for sufficient time for the water condensation or evaporation. The hygroscopic curves are represented by the area ratio (A/A_0) as a function of RH, where the 2-D projected aerosol area at a given RH (A) is divided by that before starting the humidification process (A_0). The images were processed using image analysis software (Matrox Inspector v9.0). The experiments were conducted at room temperature ($T = 22 \pm 1$ °C). Pure NaCl particles were used to verify the accuracy of the system, with DRH equal to 75.5(±0.5) % and ERH equal to 46.3 %–47.6 %.

2.3 Low Z particle EPMA measurements using SEM-EDX

The ambient aerosol particles were analyzed using low Z particle EPMA measurements with a JEOL JSM-6390 SEM equipped with an Oxford Link super atmospheric thin win-

dow (SATW) EDX detector. The analysis was conducted both before and after the hygroscopic processes to find out fields on TEM grids with well-separated particles based on their secondary electron images (SEIs; $\sim 100\,\mu m \times 100\,\mu m$ for a field) and to determine the morphology, chemical composition, and spatial distribution of the chemical elements (elemental maps), respectively. The resolution of the detector was 133 eV for Mn Kα X-rays. The point-mode and area-mode X-ray spectra and elemental maps of individual particles were recorded using Oxford Instruments INCA Energy software. An accelerating voltage of 10 kV and beam current of 0.5 nA were used, and typical measurement durations were 20 s for the point mode, 1 min for the area mode, and 5–10 min for elemental mapping.

The AXIL program was used to obtain the net X-ray intensities for chemical elements through nonlinear least squares fitting of the spectra. From these intensities, the elemental concentrations of individual particles were determined (Vekemans et al., 1994). For individual particles sitting on TEM grids, C and O concentrations were determined using a Monte Carlo calculation technique to correct for the interfering X-ray peaks of C and O emitted from the TEM grid, thus providing accurate quantification results (Geng et al., 2010). A detailed explanation of the elemental quantification procedure can be found elsewhere (Wu et al., 2019).

3 Results and discussion

3.1 Chemical composition and hygroscopic behavior of individual ambient aerosol particles

In this study, a total of 39 particles on three fields were investigated, including 24 aged or reacted SSAs with diverse mixing ratios of Cl^- and NO_3^- and 15 other particles, such as 6 aluminosilicates, 5 Ca-containing particles, 2 Fe-rich particles, an aged SiO_2, and a mixture particle of organic and $(NH_4)_2SO_4$. The mole fraction of Cl as $X_{(Na,Mg)Cl}$ in the aged or reacted SSAs was calculated based on $[Cl^-]/([Na^+]+2[Mg^{2+}])$ to determine the degree of Cl depletion in the SSA particles. Figure 2 shows the SEI of the first field containing 16 particles, where the chemical species of each particle are indicated with two exemplar X-ray spectra of aged SSAs no. 5 and no. 11, with $X_{(Na,Mg)Cl} = 0.75$ and 0.23, respectively. The elemental concentrations of all particles and their chemical species, determined by X-ray spectral analysis, are listed in Table S1 of the Supplement.

In Fig. 3, optical images obtained at different RHs during the humidification and dehydration processes and the secondary electron image (SEIs) after hygroscopic process for 16 particles on the first field are shown. Except for particle nos. 2, 4, 7, 8, and 14, the rest are aged SSAs. Optical images and the SEIs for particles on the second and third fields are provided in Figs. S1 and S2 in the Supplement, respectively. Particles were initially solid at RH 5.3 % before the hygroscopic measurement, as shown in Fig. 3a. During the humidification process, most of the SSAs showed partial deliquescence at RH 63.8 % (Fig. 3c), regardless of their aging degree, indicating the realization of the MDRH. Upon further increase in the RH, SSAs underwent full deliquescence transitions at DRH equal to 65.4 %–73.5 %, which varied for each SSA, as shown in Fig. 3d and e. During the dehydration process, almost all SSAs exhibited colored ring-type patterns (Fig. 3g and h) due to the diffraction of visible light typically observed in the presence of organic surfactants on water, indicating the presence of considerable amounts of organic species in aged SSAs. SSA droplet no. 5 crystallized at ERH 50.5 % (Fig. 3g), while the others effloresced over a lower range of ERH 46.0 % to 17.9 %. The various DRHs and ERHs indicate the different chemical compositions of SSAs.

Aluminosilicates and Fe-rich particles did not exhibit any water uptake or changes as a function of RH. Aged aluminosilicates, aged SiO_2, and some reacted Ca-containing particles showed modest growth or shrinkage continuously due to the presence of amorphous NO_3^- phases (Ahn et al., 2010). The mixture particle of organic and ammonium sulfate experienced distinct deliquescence and efflorescence. A detailed description of the hygroscopic behavior of the ambient aerosol particles is given as follows.

3.2 SSA particles

The average atomic concentrations of C, Na, Cl, N, Mg, S, K, and Ca in SSAs are listed in Table S1, with the values being 43.0(±7.2) %, 13.6(±4.6) %, 8.0(±6.6) %, 7.9(±2.3) %, 1.5(±0.4) %, 0.8(±0.3) %, 0.3(±0.1) %, and 0.3(±0.1) %, respectively. The elemental analysis of the SSAs indicates that they consist primarily of Na^+, Mg^{2+}, Cl^-, NO_3^-, and organic species. The elemental concentration of N is significantly higher than that of S, and the elemental ratio of S and Na in the ambient SSAs collected from our samples closely resembles that of seawater ([S]/[Na] = 0.06; Haynes, 2015). As a result, the SSAs are considered to contain more nitrate due to the rapid reaction with NO_x/HNO_3, as opposed to sulfate. As the SSAs become more aged or reacted, their mole fractions of Cl^- relative to Na^+ and Mg^{2+} decrease, while their mole fractions of NO_3^- increase. Although the aged or reacted SSAs are a complicated multicomponent system as a fraction of ambient aerosols, the (Na, Mg)(Cl, NO_3) mixture system is considered to be an inorganic surrogate system useful for understanding their hygroscopic behavior. The AIOMFAC model predicts the eutonic compositions of the Na(Cl, NO_3) and (Na, Mg)(Cl, NO_3) mixture systems as $X_{NaCl} = 0.38$ and $X_{(Na,Mg)Cl} = 0.46$, respectively. The mole fraction of Cl in the eutonic compositions of the inorganic component of the aged SSAs would be around 0.4. Thus, the SSAs can be classified as Cl rich or Cl depleted, depending on whether their $X_{(Na,Mg)Cl}$ values are greater or less than 0.4, respectively.

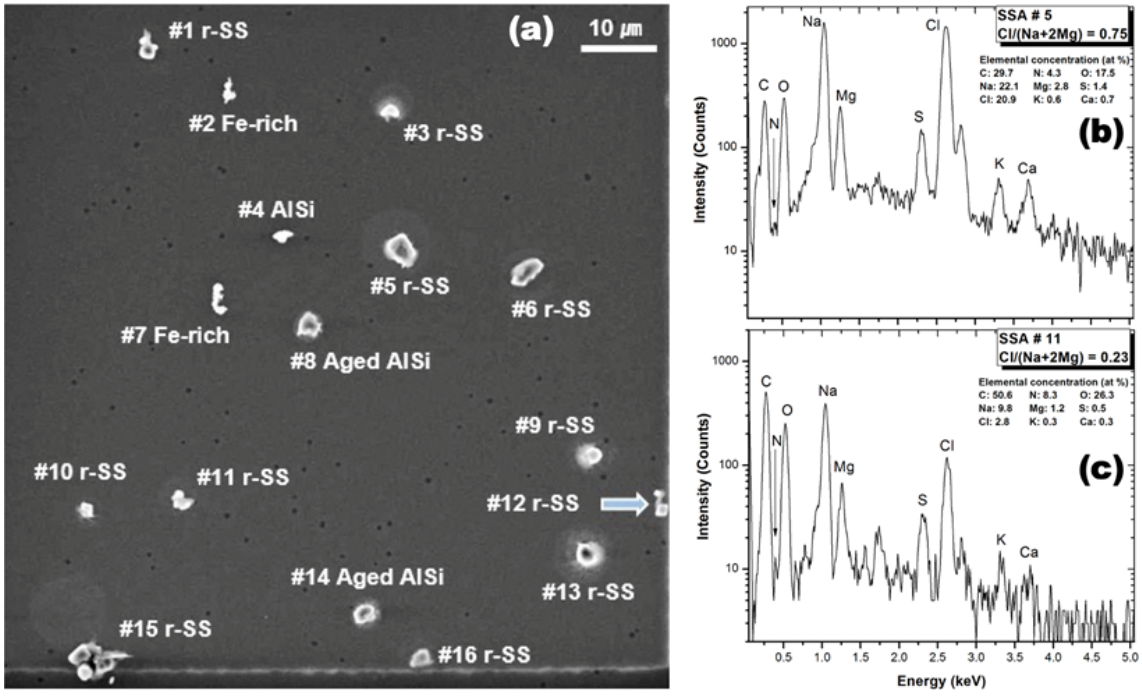

Figure 2. **(a)** Secondary electron image (SEI) of the first field containing 16 particles and X-ray spectra of **(b)** Cl-rich and **(c)** Cl-depleted aged SSAs (particle nos. 5 and 11, respectively). In this image, aged SSAs, Fe-containing particles, and aluminosilicates are denoted as "r-SS", "Fe rich", and "AlSi", respectively.

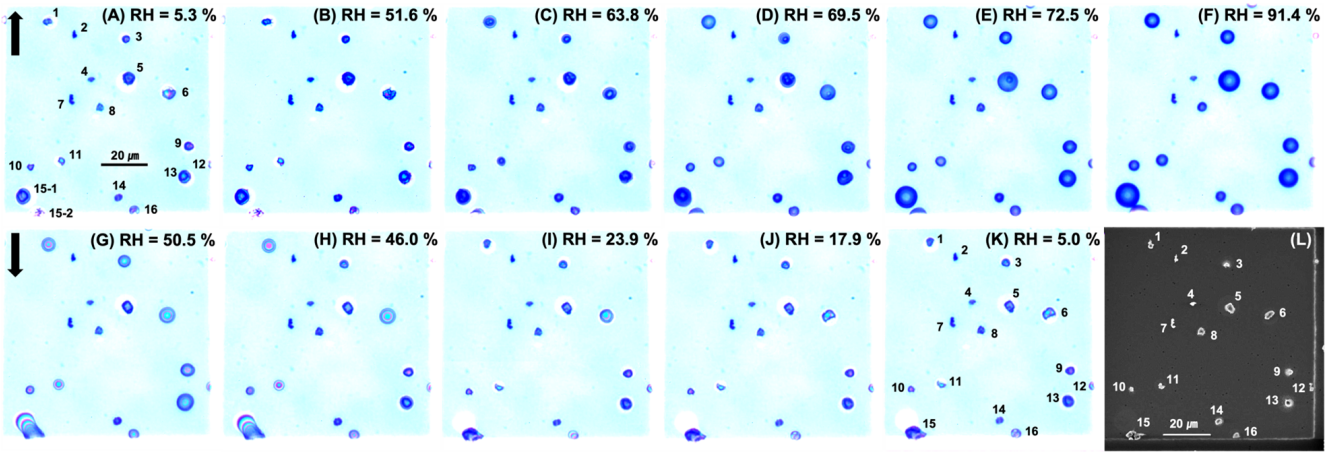

Figure 3. Optical images of the first field on TEM grid during humidifying (**a–f**, ↑) and dehydration (**g–k**, ↓) processes and the SEI of the same field (**l**).

3.2.1 Cl-rich SSAs

Figure 4 displays the projected 2-dimensional (2-D) area ratio and optical images for Cl-rich SSAs that are numbered 5 and 19 (Fig. 4a and d, respectively) and the 2-D area ratio of humidification (Fig. 4b and e) and dehydration (Fig. 4c and f) for the two SSAs as a function of RH. For SSAs that are numbered 5 and 19, the mole fraction of chloride $X_{(Na,Mg)Cl}$ was calculated to be 0.75 and 0.72, respectively. In addition, the figure also includes the (Na, Mg)(Cl, NO_3) particle with $X_{(Na,Mg)Cl} = 0.75$ for comparison.

During the humidification process, the SSAs that are numbered 5 and 19 initially remained constant in size until RH reached around 30 %, after which they gradually increased in size. This behavior is also consistent with the (Na, Mg)(Cl, NO_3) system (Fig. 4b and e), suggesting that $MgCl_2 \cdot 6H_2O$ (DRH 33.3 %) or the Mg^{2+}-rich eutonic part may have undergone water absorption (Gupta et al., 2015a; Zieger et

al., 2017). However, the deliquescence transitions were not as distinct as those in particles with $X_{(Na,Mg)Cl} = 0.25$ and 0.5 generated from (Na, Mg)(Cl, NO_3) mixture solutions (see Fig. S3). The size increase was followed by a shrinkage until RH 60.5 %, due to the structural rearrangement in the remaining undissolved salt mixture crystals. Structural rearrangements are commonly observed after preliminary absorption of water at RHs just before the prompt deliquescence transition (Ahn et al., 2010; Gupta et al., 2015a, b; Mikhailov et al., 2009). At first, DRH is equal to 63.8 %, and a partial droplet-like shape appeared in the particle morphology, although there was no significant change in the 2-D area ratio. Clear final deliquescence transitions were observed in both SSAs that are numbered 5 and 19 at DRH values of 73.5 % and 72.9 %, respectively, due to the dissolution of the remaining solid NaCl moiety in these Cl-rich particles. The measured DRHs of SSAs that are numbered 5 and 19 were closer to the final DRHs calculated for the Na(Cl, NO_3) system, using the AIOMFAC model (Fig. 6), and higher than the calculated and measured ones in the (Na, Mg)(Cl, NO_3) particles (Figs. 4b, e and 6). These observations for the Cl-rich SSAs suggest that most of the Mg^{2+} salts ($MgCl_2{\cdot}6H_2O$ with DRH 33.3 % and $Mg(NO_3)_2$ with DRH 52 %) have either already dissolved at low RHs or undergone complexation with organic moieties (Eom et al., 2016), and the remaining NaCl and $NaNO_3$ moieties drove the deliquescence transition. The hygroscopic growth of both SSAs that are numbered 5 and 19 was much smaller than that of the (Na, Mg)(Cl, NO_3) system (Fig. 4b and e) when RH was raised to 91.4 %, indicating the presence of a partitioning hydrophobic layer composed of organic surfactants that covered the aqueous salt droplets and inhibited water uptake (Bertram et al., 2018; Cochran et al., 2016; Eom et al., 2016; Lee et al., 2020).

During the dehydration process, as RH decreased from $\sim$ 91 % to $\sim$ 5 %, both the SSA droplets showed a continuous shrinkage in size before their efflorescence. However, the rate of shrinkage was much smaller than that of pure inorganic surrogates, such as the (Na, Mg)(Cl, NO_3) system with $X_{(Na,Mg)Cl} = 0.75$ (Fig. 4c and f), indicating that the hydrophobic surfactant layers covering the aqueous salt droplets potentially impeded the water evaporation. SSAs that are numbered 5 and 19 showed one clear efflorescence transition at RH 50.5 % and 45.0 %, respectively (Fig. 4a and d). Interestingly, SSA no. 5 ($X_{(Na,Mg)Cl} = 0.75$) underwent a sharp decrease in size from RH 50.9 % to 50.5 %, which is considerably higher than the ERH range of $\sim$ 45 % to 47 % for pure NaCl particles (Ahn et al., 2010; Eom et al., 2014; Martin, 2000) and the first ERHs of either Na(Cl, NO_3) (Fig. 7) or (Na, Mg)(Cl, NO_3) (Figs. 4c and 7) systems. On the other hand, SSA no. 19 ($X_{(Na,Mg)Cl} = 0.72$) first showed a small decrease in size at RH 63.8 % to 60.8 %, which is not a typical efflorescence transition, followed by a sharp decrease in size at RH 45.8 % to 45.0 %, which is on the lower side of the ERH range for pure NaCl and slightly higher than the first ERHs of Na(Cl, NO_3) and (Na, Mg)(Cl, NO_3) systems (Figs. 4f and 7). The higher ERH at RH 50.5 % in SSA no. 5 indicates the heterogeneous efflorescence of the NaCl moiety, while the ERH 45.0 % in SSA no. 19 suggests the homogeneous nucleation of the NaCl moiety. Both SSA droplets showed just one decisive efflorescence transition at their ERHs, indicating the co-crystallization of most aqueous inorganic salt moieties along with NaCl, pointing towards the likelihood that the SSAs with more complicated chemical compositions than the (Na, Mg)(Cl, NO_3) mixture aerosols contain chemicals which can act as seeds, such as (Na, Ca)SO_4 crystals, for the complete crystallization at the efflorescence transition. These observations are substantiated by the distribution of S and O at the center and edge of the NaCl moiety in the X-ray maps obtained from the effloresced SSA particles that are numbered 5 and 19, respectively (Fig. S4; Li et al., 2014; Gupta et al., 2015a). The apparent (not so sharp) decrease in size of SSA no. 19 at RH 63.8 % to 60.8 % could be attributed to (i) the sudden shrinkage of viscous organic moieties covering the aqueous salt droplet or (ii) inhibited or slow water loss, probably due to a kinetic barrier to crystallization from amorphous- or gel-forming moieties such as $MgSO_4/Mg(NO_3)_2/(CH_3SO_3)_2(Mg, Ca)$ (Liu and Laskin, 2009; Xiao et al., 2008; Zhang et al., 2004; Zhao et al., 2006). The other reason could be that (iii) a phase transition, such as heterogeneous efflorescence, had occurred, but the presence of viscous moieties (organics or Mg^{2+}-organic complex) affected the relative 2-D size decrease on the TEM grid substrate.

3.2.2 Equimolar and Cl-depleted SSAs

Figure 5 shows the plots of the projected 2-D area ratio and optical images for an equimolar SSA (no. 23; Fig. 5a) and a Cl-depleted SSA (no. 11; Fig. 5d) and the 2-D area ratio of humidification (Fig. 5b and e) and dehydration (Fig. 5c and f) for the two SSAs as a function of RH. The calculated mole fractions of chloride $X_{(Na,Mg)Cl}$ for the SSAs that are numbered 23 and 11 are 0.52 and 0.23, respectively. Figure 5 also includes the (Na, Mg)(Cl, NO_3) particles with $X_{(Na,Mg)Cl} = 0.5$ and 0.25 for comparison.

During the humidification process, both SSAs that are numbered 23 and 11 remained relatively constant until RH $\simeq$ 50 %, unlike the (Na, Mg)(Cl, NO_3) system, which is probably due to the decreased concentration of $MgCl_2 \cdot 6H_2O$. The particle size then began to shrink until RH $\simeq$ 59 %. Both SSAs exhibited two distinct deliquescence transitions. Partial deliquescence transitions occurred at RH $\simeq$ 63.8 %, which is the MDRH for the mixture of soluble moieties in the ambient SSAs and was reported for the first time. Both SSAs exhibited two clear deliquescence transitions. The observed and AIOMFAC-calculated MDRHs of the Na(Cl, NO_3) system are $\sim$ 68 %, while the AIOMFAC-calculated second MDRH for the (Na, Mg)(Cl, NO_3) system is 66.5 % after the dissolution of $MgCl_2{\cdot}6H_2O$ at the calculated first MDRH of $\sim$ 34 %, as shown in Fig. 6. This indicates that the eutonic component

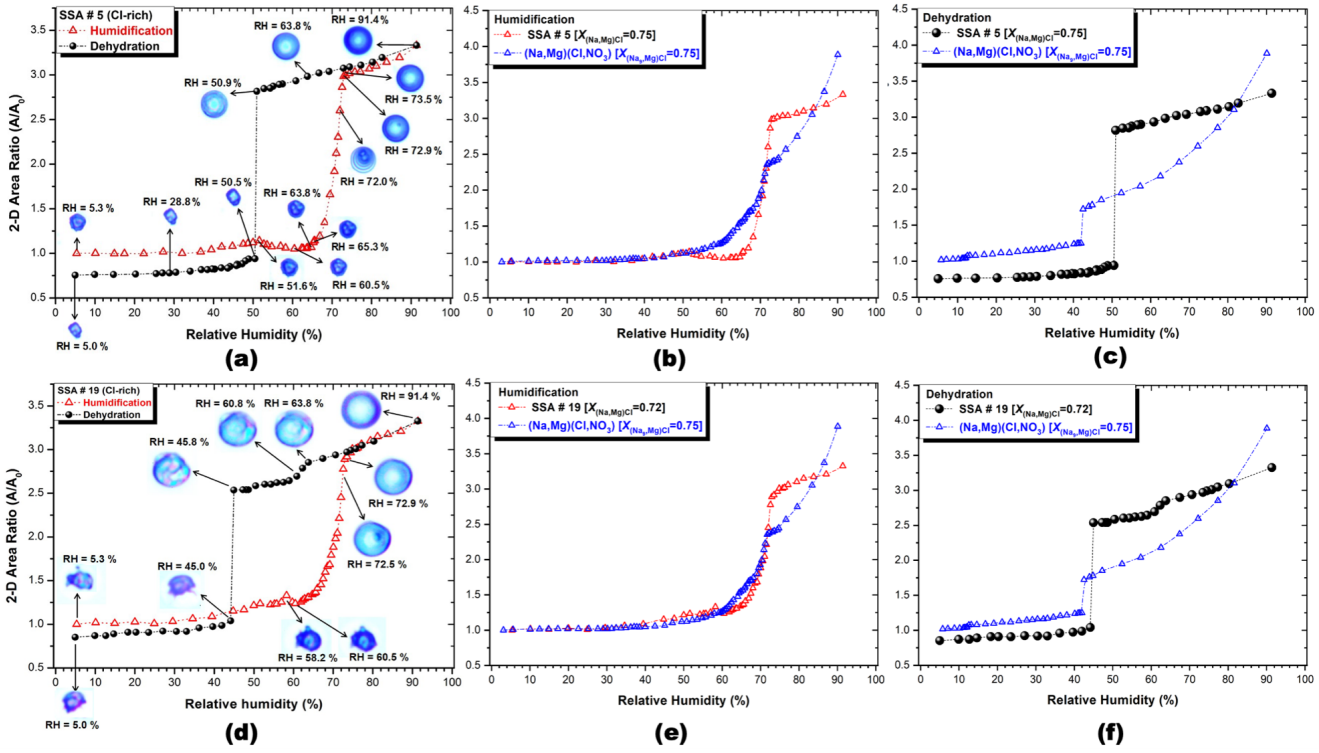

Figure 4. The 2-D area ratio plot and optical images of Cl-rich SSAs that are numbered 5 and 19 **(a, d)**. The 2-D area ratio plots of humidification **(b, e)** and dehydration **(c, f)** for the SSAs and (Na,Mg)(Cl, NO_3) particles as a function of RH.

in the ambient SSAs, with a lower MDRH of 63.8 %, is composed of NaCl, $NaNO_3$, $Mg(NO_3)_2$, and some other minor, less-soluble moieties. The mutual deliquescence transition was more distinct in Cl-depleted SSAs than in Cl-rich SSAs, suggesting that the eutonic component in the ambient SSAs is richer with other salts compared to NaCl. As RH increased further, both SSAs that are numbered 23 and 11 underwent final deliquescence transitions at DRH values of 69.5 %. The observed DRH for SSA no. 23 ($X_{(Na,Mg)Cl} = 0.52$) is closer to the final DRH calculated from AIOMFAC for the pure NaCl moiety in the Na(Cl, NO_3) system (Fig. 6) and higher than the AIOMFAC-calculated final DRH for pure NaCl moiety in the (Na, Mg)(Cl, NO_3) system (Figs. 5b and 6). The observed DRH for SSA no. 11 ($X_{(Na,Mg)Cl} = 0.23$) is lower than the AIOMFAC-calculated final DRH (Fig. 6) for the pure $NaNO_3$ moiety in the Na(Cl, NO_3) system (Gupta et al., 2015b) and close to the AIOMFAC-calculated final DRH for pure $NaNO_3$ moiety in the (Na, Mg)(Cl, NO_3) system (Figs. 5e and 6). The observation of Cl-depleted SSAs during humidification suggests that a (Na, Mg)(Cl, NO_3)-dominant composition drives the deliquescence transition. As RH increased further, the hygroscopic growth of both SSAs that are numbered 23 and 11 was stunted when compared to the (Na, Mg)(Cl, NO_3) mixture systems (Fig. 5b and e), likely due to the presence of hydrophobic surfactants covering the aqueous salt droplet.

During the dehydration process, both SSAs that are numbered 23 and 11 showed slower rates of shrinkage compared to the (Na, Mg)(Cl, NO_3) mixture systems (Fig. 5c and f), suggesting inhibition of water evaporation due to surface hydrophobic organic moieties. The diffraction patterns at the aqueous salt droplet–organic surfactant interface were more prominent in the form of colored and/or ring-like patterns for equimolar and Cl-depleted SSAs (Fig. 5a and d), indicating that the hydrophobic organic film may become thicker or that the concentration of organic surfactants may increase with aging. During dehydration, SSA no. 23, which is equimolar or slightly Cl rich, showed one sharp transition at RH 44.1 % to 43.6 % and a gradual decrease in size thereafter until RH 30.7 %, which is not considered to be an efflorescence transition (Fig. 5a). The distinct ERH of 43.6 % observed for SSA no. 23 was higher than the first ERHs of both Na(Cl, NO_3) and (Na, Mg)(Cl, NO_3) systems (Figs. 5c and 7), indicating the possible homogeneous efflorescence of NaCl along with other salts on crystalline seeds such as (Ca, Na)SO_4 (Pósfai et al., 1995; Semeniuk et al., 2007; Wise et al., 2007), as shown in the X-ray maps in Fig. S5a. The remaining metastable amorphous- or gel-type NO_3^- moieties and $MgSO_4 \cdot xH_2O$ may be responsible for the gradual decrease in size after the efflorescence transition (Li et al., 2016). Cl-depleted SSA no. 11 showed two clear efflorescence transitions at RH 44.1 % to 39.6 % and 24.6 % to

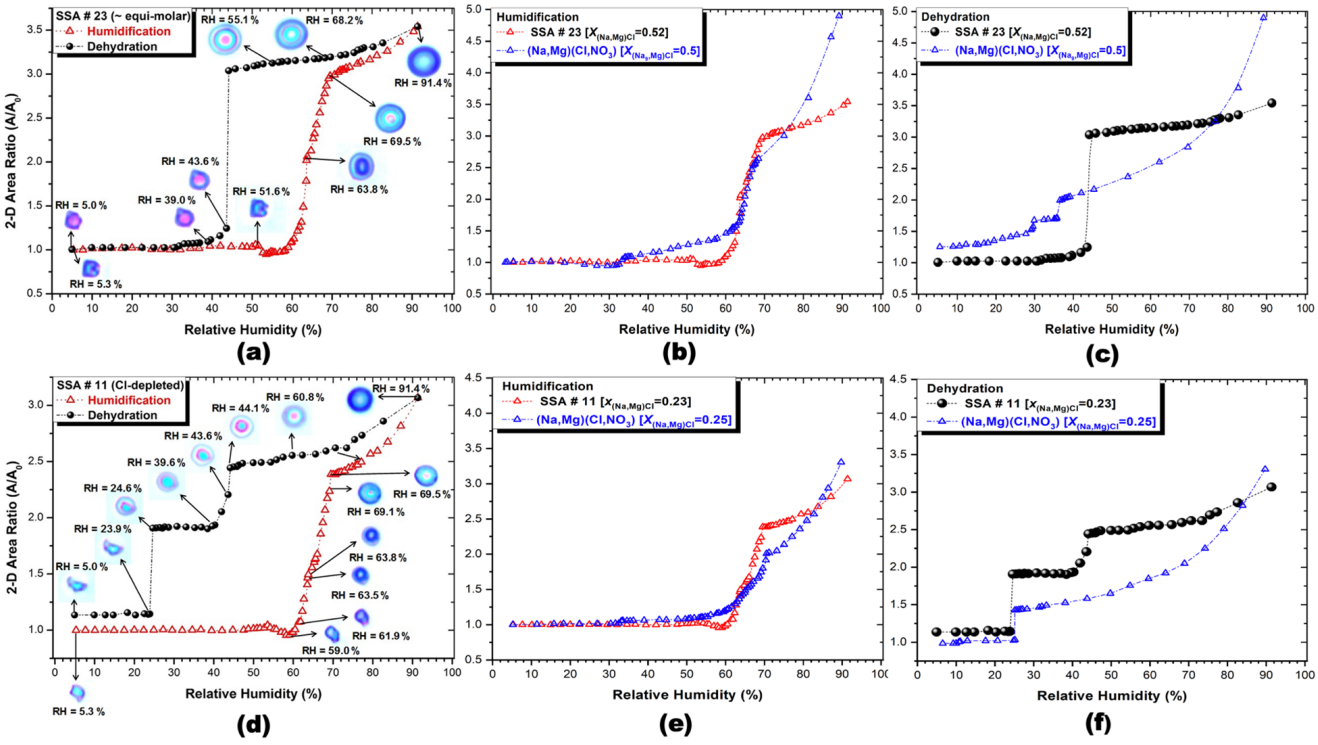

Figure 5. The 2-D area ratio plot and optical images of an equimolar SSA (no. 23) and a Cl-depleted SSA (no. 11) **(a, d)**. The 2-D area ratio plots of humidification **(b, e)** and dehydration **(c, f)** for the SSAs and (Na, Mg)(Cl, NO_3) particles as a function of RH.

23.9 %, as shown in Fig. 5d. The first ERH of 39.6 % measured for SSA no. 11 was also higher than the ERHs for both Na(Cl, NO_3) and (Na, Mg)(Cl, NO_3) systems, while the second ERH of 23.9 % was close to and lower than the ERH range for pure NaCl in (Na, Mg)(Cl, NO_3) and Na(Cl, NO_3) systems, respectively (Figs. 5f and 7). The observations for Cl-depleted SSA no. 11 suggest that the first ERH was most probably due to the heterogeneous crystallization of the dominant $NaNO_3$ and/or $Mg(NO_3)_2$ on mixed cation sulfate crystalline seeds such as (Ca, Na)SO_4, while NaCl continued to homogeneously nucleate until the second ERH, where it crystallized at the center or core of the particle (Woods et al., 2013), as shown in the X-ray maps in Fig. S5b.

3.2.3 Phase diagrams of ambient SSAs in correlation with Na(Cl, NO_3) and (Na, Mg)(Cl, NO_3) surrogate systems

The phase diagrams of ambient SSAs in correlation with Na(Cl, NO_3) and (Na, Mg)(Cl, NO_3) surrogate systems can show the relationship between the observed deliquescence and efflorescence behavior of the ambient SSAs and those of the two surrogate systems. The ambient SSAs have more complex compositions, but the simpler Na(Cl, NO_3) and (Na, Mg)(Cl, NO_3) surrogate systems can help to identify the dominant salts and their behavior in the ambient SSAs. For example, the observation of Cl-depleted SSAs during humidification suggests that a (Na, Mg)(Cl, NO_3)-dominant composition drives the deliquescence transition. This information can be useful in helping to understand the hygroscopic properties and behavior of atmospheric aerosols.

Deliquescence-phase diagram

Figure 6 shows the experimentally measured DRHs for the ambient SSA particles and those of the (Na, Mg)(Cl, NO_3) and Na(Cl, NO_3) systems calculated from the AIOMFAC model and plotted as a function of the mole fraction of chloride, namely $f(X_{(Na,Mg)Cl}$ or $X_{NaCl})$.

The first MDRH of the (Na, Mg)(Cl, NO_3) system, which was calculated from AIOMFAC, is 34.2 %, and the MDRH measured in laboratory-generated (Na, Mg)(Cl, NO_3) particles is $\sim$ 33.4 % (Fig. S3). These values are attributed to the dominant $MgCl_2 \cdot 6H_2O$ eutonic component (Gupta et al., 2015a). In some Cl-rich SSAs, a gradual increase in size and a change in morphology were observed at RH $\simeq$ 33 %, indicating that they were in the partial aqueous phase (Fig. 4a and d). It is also possible that the gradual water uptake observed in SSAs at low RHs is due to amorphous inorganic moieties such as $MgSO_4 \cdot xH_2O$ (Xiao et al., 2008; Zhao et al., 2006) and $Mg(NO_3)_2 \cdot xH_2O$ (Zhang et al., 2004), and/or water-soluble secondary organics such as carboxylate salts

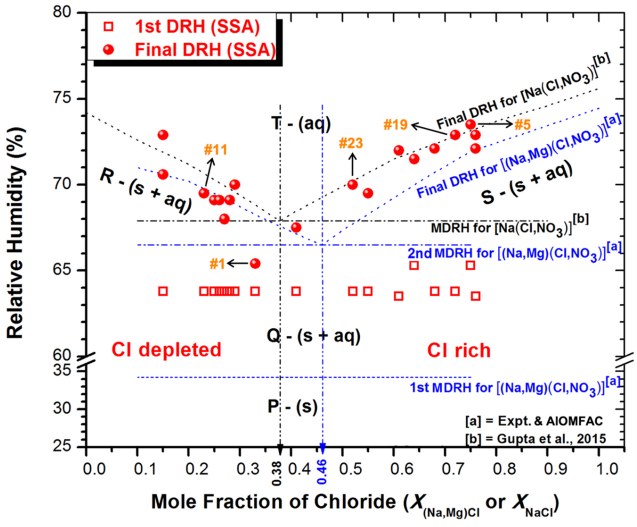

Figure 6. DRHs of ambient SSAs and (Na, Mg)(Cl, NO_3) and Na(Cl, NO_3) systems calculated from AIOMFAC plotted against the mole fraction of chloride [$X_{(Na,Mg)Cl}$ or X_{NaCl}]. Major chemical components in each phase are as follows: P – all in solid phase; Q – aqueous eutonic components plus NaCl and (Na, Mg, Ca)(NO_3, SO_4, and organics) in solid phase; R – $NaNO_3$ and (Ca, Na)SO_4 in solid-phase plus aqueous eutonic components; S – NaCl and (Ca, Na)SO_4 in solid-phase plus aqueous eutonic components; T – aqueous phase for most components; vertical black line – a eutonic composition of Na(Cl, NO_3) system; and vertical blue line – a eutonic composition of (Na, Mg)(Cl, NO_3) system.

formed due to reactions of the (Na, Mg)Cl species with dicarboxylic acids, which are ubiquitous in the marine boundary layer (Ghorai et al., 2014; Laskin et al., 2012; Li et al., 2021). Wise et al. (2009) reported that ambient SSAs started changing in morphology at 36(±15) % RH.

For the (Na, Mg)(Cl, NO_3) system, the eutonic composition is $X_{(Na,Mg)Cl} = 0.46$, with a second MDRH of 66.5 %, calculated from AIOMFAC, and a measured value of ∼ 66.6(±0.4) % in the laboratory-generated (Na, Mg)(Cl, NO_3) particles (Fig. S3). For the Na(Cl, NO_3) system, the eutonic composition is $X_{NaCl} = 0.38$, with the MDRH of 67.9 %, as calculated from AIOMFAC, and a measured value of ∼ 67.9(±0.3) % in the laboratory-generated particles (Gupta et al., 2015b). The observed MDRH of 63.8(±0.3) % for the ambient SSAs (Fig. 6) is slightly lower than those of the Na(Cl, NO_3) and (Na, Mg)(Cl, NO_3) mixture systems, indicating that the eutonic component in the mutual deliquescence transition may be Na(Cl, NO_3) rich, with minor concentrations of other soluble salt moieties, as the MDRH of salt mixtures is generally lower than individual salt DRHs (Wexler and Seinfeld, 1991). It is less likely that Na_2SO_4 or CH_3SO_3Na are major components of the eutonic component in these ambient SSAs, as they have much higher MDRHs (i.e., MDRHs 84.0 % for Na(Cl, SO_4) and 71 % for Na(Cl, CH_3SO_3); Chang and Lee, 2002; Liu and Laskin, 2009; Liu et al., 2011). The lowest final DRH measured for SSA no. 1 with $X_{(Na,Mg)Cl} = 0.33$ is at RH 65.4 % (Fig. 6), which is close to the observed MDRH of 63.8(±0.3) %, suggesting that the eutonic component likely has a chloride mole fraction within the range of $X_{(Na,Mg)Cl} \simeq 0.30$–$0.40$. Interestingly, Wise et al. (2009) reported rounding in particle morphology at RH 65(±4) %, which is close to the observed MDRH but was not confirmed as such, since only four ambient SSA particles were studied.

The final DRHs in both (Na, Mg)(Cl, NO_3) and Na(Cl, NO_3) systems are solely determined by the solid salt remaining after the mutual deliquescence of the eutonic component. Figure 6 clearly shows that for the Cl-rich SSA particles with $X_{(Na,Mg)Cl} > 0.40$, which contain more NaCl than the eutonic composition, the final DRH values (∼ 67.5 %–73.5 %) approached the DRH of pure NaCl salt (∼ 75.3 % at 298 K) as the chloride concentration increased. Similarly, for the Cl-depleted particles with $X_{(Na,Mg)Cl} < 0.40$, the final DRH values (∼ 65.4 %–72.9 %) approached that of pure $NaNO_3$ salt (∼ 74 % at 298 K) as the chloride concentration decreased.

The chemical components of each phase in the ambient SSAs during the humidification process are not well known; therefore, five possible single and/or mixed phases are notated as alphabet letters (P, Q, R, S, and T), and the possible major chemical components in each phase (s is for solid; aq is for aqueous) are listed as follows:

i. P-(s) is where all components are mixed in the solid phase at RH $\lesssim$ 33 %–35 % at all mole fractions of chloride.

ii. Q-(s plus aq) indicates a mixed phase comprising possibly aqueous $MgCl_2 \cdot 6H_2O$-dominant eutonic components plus solid NaCl, the (Na, Mg, Ca)(NO_3, SO_4) mixture, and organics between RH $\simeq$ 33 % and the first clear MDRH of ∼ 63.8 %.

iii. R-(s plus aq) indicates a mixed phase comprising solid $NaNO_3$ and (Ca, Na)SO_4 plus aqueous eutonic components rich in Na(Cl, NO_3) and Mg(NO_3, SO_4, and organics) between RH 63.8 % and the final DRHs for $X_{(Na,Mg)Cl} < 0.40$, i.e., Cl-depleted SSAs.

iv. S-(s plus aq) indicates a mixed phase comprising solid NaCl and (Ca, Na)SO_4 plus aqueous eutonic components rich in Na(Cl, NO_3) and Mg(Cl, NO_3, SO_4, and organics) between the RH 63.8 % and final DRHs for $X_{(Na,Mg)Cl} > 0.40$, i.e., Cl-rich SSAs.

v. T-(aq) indicates the aqueous phase for most components, including NaCl, $NaNO_3$, and Mg(Cl, NO_3, SO_4, and organics) above the measured final DRHs at all mole fractions of chloride, while (Ca, Na)SO_4 should remain in the crystalline solid phase and does not take part in the deliquescence transitions in the measured RH range.

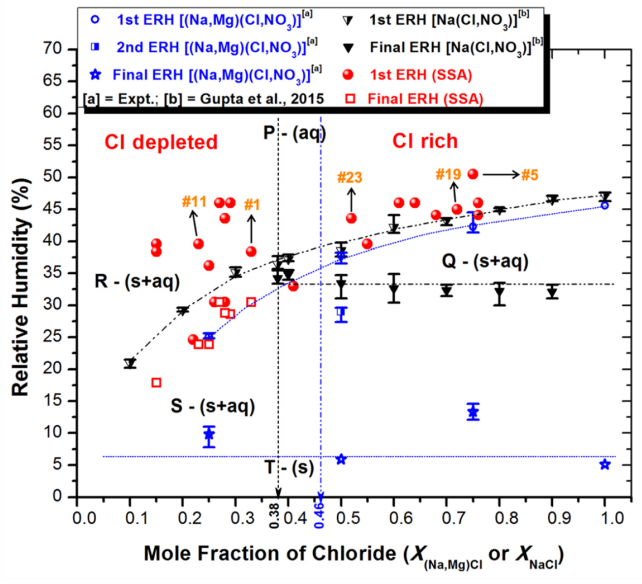

Figure 7. ERHs of ambient SSAs and those experimentally determined for (Na, Mg)(Cl, NO_3) and Na(Cl, NO_3) systems plotted against the mole fraction of chloride [$X_{(Na,Mg)Cl}$ or X_{NaCl}]. Major chemical components in each phase are as follows: P – almost all components in aqueous phase; Q – NaCl and other heterogeneously crystallized moieties in solid-phase plus aqueous nucleating species like $(Mg \cdot xH_2O)^{2+}$ and $Cl^-/NO_3^-/SO_4^{2-}$; R – heterogeneously crystallized (Na, Mg)$NO_3 \cdot xH_2O$ on crystalline (Ca, Na)$SO_4(xH_2O)$ seeds plus aqueous NaCl and other moieties; S – solid (Na, Mg, Ca)(NO_3, SO_4)$\cdot xH_2O$ and homogeneously crystallized NaCl plus aqueous or amorphous $(Mg \cdot xH_2O)^{2+}$ and NO_3^-/SO_4^{2-}, and other minor species; T – all in solid phase; vertical black line – a eutonic composition of Na(Cl, NO_3) system; and vertical blue line – a eutonic composition of (Na, Mg)(Cl, NO_3)system.

Efflorescence-phase diagram

The experimentally measured ERHs for the ambient SSA particles and those of (Na, Mg)(Cl, NO_3) and Na(Cl, NO_3) systems are plotted as a function of the mole fraction of chloride ($f(X_{(Na,Mg)Cl}$ or $X_{NaCl})$) in Fig. 7.

The first ERH values decrease from 44.5 % to 24.8 % and from 47.1 % to 20.2 % with decreasing mole fractions of chloride for $X_{(Na,Mg)Cl} = 0.75$ to 0.25 in the (Na, Mg)(Cl, NO_3) and $X_{NaCl} = 0.9$ to 0.1 in the Na(Cl, NO_3) systems, respectively (Gupta et al., 2015b; Woods et al., 2013). This suggests that the first efflorescence transitions in the Na(Cl, NO_3) and (Na, Mg)(Cl, NO_3) mixture systems are solely due to the homogeneous nucleation of NaCl for both Cl-rich and Cl-depleted particles and that the amorphous (Na, Mg)NO_3 species cannot undergo homogeneous crystallization even at high supersaturation (Kim et al., 2012; Zhang et al., 2004). In the case of Cl-rich ($X_{(Na,Mg)Cl} > 0.40$) ambient SSAs, the first ERHs systematically decreased, ranging from 50.5 % to 33.0 %, due to the homogeneous nucleation of NaCl for most particles. However, for a few particles, such as SSA no. 5 (Fig. 4a; ERH 50.5 %), NaCl underwent heterogeneous crystallization on the mixed cation sulfate (Ca, Na)SO_4 crystalline seeds, resulting in higher ERH values. On the other hand, in Cl-depleted ($X_{(Na,Mg)Cl} < 0.40$) SSA particles, the first ERH values ranged from 46.0 % to 24.6 % as a random set of values higher than the first ERHs in Na(Cl, NO_3) and (Na, Mg)(Cl, NO_3) mixture systems (Fig. 7), indicating the heterogeneous crystallization of the richer (Na, Mg)NO_3 moieties on the mixed cation sulfate crystalline seeds for most particles.

The second or final ERH in the Na(Cl, NO_3) system was only observed for Cl-rich particles ($X_{NaCl} > 0.38$) due to the mutual efflorescence of the eutonic component ($X_{NaCl} = 0.38$) at MERH $\simeq$ 30.0 %–35.5 %, while no second ERH was recorded for Cl-depleted particles, as $NaNO_3$ heterogeneously crystallized simultaneously on the homogeneously nucleated NaCl seeds (Gupta et al., 2015a). For the (Na, Mg)(Cl, NO_3), a second ERH $\simeq$ 29.6 %–27.4 % was only observed for $X_{(Na,Mg)Cl} = 0.5$ among the three compositions measured (Fig. S3), probably due to the stochastic heterogeneous crystallization of the Na(Cl, NO_3)-rich eutonic moiety on the NaCl seed. On the other hand, the typical transitions from 30.5 % to 17.9 % for the second or final ERH in ambient SSAs were only observed for Cl-depleted particles with decreasing chloride concentration (i.e., $X_{(Na,Mg)Cl} \simeq 0.33$ to 0.15), indicating the homogeneous nucleation of NaCl followed by the assumed simultaneous heterogeneous crystallization of remaining aqueous salt moieties such as Mg(SO_4, NO_3).

In the laboratory-generated (Na, Mg)(Cl, NO_3), particles with different mole fractions of chloride, i.e., $X_{(Na,Mg)Cl} = 0.25$, 0.5, 0.75 (Fig. S3), and 1.0 (Gupta et al., 2015a), clear final ERHs, or MERHs were observed at low RHs ranging from 11.0 % to 5.1 % ($X_{(Na,Mg)Cl} = 0.25$, 0.5, and 1.0) and 14.6 % to 12.1 % ($X_{(Na,Mg)Cl} = 0.75$), probably due to the crystallization of the dominant eutonic component of $MgCl_2 \cdot 4H_2O$ and $MgCl_2 \cdot 6H_2O$, respectively. However, such low values of ERHs were not observed in the ambient SSAs, possibly because the concentrations of $MgCl_2 \cdot xH_2O$ were too small to be detected by the optical-microscopy-derived 2-D area ratio. On the other hand, the very gradual shrinkage observed in ambient SSAs at low RHs may be due to the presence of amorphous Mg(NO_3, SO_4)$\cdot xH_2O$ moieties, which were present in some particles (e.g., SSAs that are numbered 5, 19, and 23 in Figs. 4a, d, and 5a).

Considering the possibility of the water content at low RHs during the dehydration process (Cziczo et al., 1997; Gupta et al., 2015a; Tang et al., 1997), the ambient SSAs can be divided into five potential phases, denoted as alphabet letters (P, Q, R, S, T), based on the presence of different chemical components and their states at different relative humidities (RHs) and the major chemical components in each phase (s is for solid; aq is for aqueous), are listed as follows:

i. P-(aq), which has almost all components, including NaCl, $NaNO_3$, and Mg(Cl, NO_3, SO_4, and organics), that are mixed in the aqueous phase at RH $\gtrsim$ 55 % for all mole fractions of chloride. The (Ca, Na)SO_4 should remain in the crystalline solid phase, as it does not take part in the phase transitions within the measured RH range.

ii. Q-(s plus aq), which is a mixed phase including solid NaCl and other heterogeneously crystallized moieties plus aqueous nucleating species like $(Mg \cdot xH_2O)^{2+}$ and $Cl^-/NO_3^-/SO_4^{2-}$ at RHs < 50.5 % in Cl-rich SSAs ($X_{(Na,Mg)Cl} > 0.40$).

iii. R-(s plus aq), which is a mixed phase including heterogeneously crystallized (Na, Mg)$NO_3 \cdot xH_2O$ on crystalline (Ca, Na)$SO_4(xH_2O)$ seeds plus aqueous NaCl and other moieties between the first ERHs from 46.0 % to 24.6 % and final ERHs from 30.5 % to 17.9 % for Cl-depleted SSAs ($X_{(Na,Mg)Cl} < 0.40$).

iv. S-(s plus aq), which is a mixed phase including solid (Na, Mg, Ca)(NO_3, SO_4)$\cdot xH_2O$ and homogeneously crystallized NaCl plus aqueous or amorphous $(Mg \cdot xH_2O)^{2+}$ and NO_3^-/SO_4^{2-} and other minor species below final ERHs from 30.5 % to 17.9 % for Cl-depleted SSAs ($X_{(Na,Mg)Cl} < 0.40$).

v. T-(s), where all components are mixed in solid phase at RH $\simeq$ 14.6 %–5.0 % for all mole fractions of chloride. Amorphous- or gel-forming Mg(NO_3, SO_4)$\cdot xH_2O$ show gradual water loss, while only a small amount of $MgCl_2 \cdot xH_2O$ is expected to crystallize.

3.3 Non-SSA particles

Generally, mineral particles such as aluminosilicates and calcium carbonate tend to have difficulty absorbing water and growing in size with increasing RH. However, these particles can become hygroscopic after a reaction with NO_x and SO_2 in the presence of water and/or mixing with SSAs. Particle no. 14 shown in Fig. 8 is a highly aged aluminosilicate that has mixed with an SSA moiety, probably with (Na, Mg)(Cl, NO_3) and organic species, as confirmed using X-ray spectrum. Clear deliquescence and efflorescence transitions are observed in the gradual growth and shrinkage of particle no. 14, mainly due to the SSA part, and the growth of the aged aluminosilicate is certainly smaller than the SSA at maximum RH. Particle no. 20 shown in Fig. S6 is a reacted Ca-containing particle with nitrate showing the gradual change in size during humidification and dehydration processes, following the hygroscopic property reported before (Ahn et al., 2010). Particle no. 36 is a typical ammonium sulfate mixed with organic species, as shown in Fig. S7, and the major chemical components of particle no. 36 are C, N, O, and S. The particle first showed a partial deliquescence transition at RH 67.5 %, which may be the MDRH for the mixture of ammonium sulfate and organic species. Upon a further increase in RH, the particle absorbed more moisture and fully dissolved at RH 77.1 %, which is slightly lower than the DRH of pure ammonium sulfate particles (Wu et al., 2019). During the dehydration process, particle no. 36 showed a slower rate of shrinkage than ammonium sulfate particles, indicating the inhibition of water evaporation due to surface hydrophobic organic moieties and effloresced at RH 27.6 %, which is lower than the ERH of ammonium sulfate particles (Wu et al., 2019). Some particles, such as reacted Ca-containing particles (no. 17 and no. 25) and an aged SiO_2 particle (no. 37), exhibit partial dissolution, as shown in Figs. S8 and S9. The 2-D area ratio of particle no. 17 at maximum RH is larger than that of particle no. 25, indicating the existence of more hygroscopic components in particle no. 17. Particle no. 37 showed a gradual increase and decrease, with partial dissolution only on the right side of particle, possibly due to the reacted Ca-containing one with nitrate moiety. The observation of the hygroscopic behavior of particles having partial growth suggests that a small content of hygroscopic chemical species can control the hygroscopic behavior of particles with major non-hygroscopic species. On the other hand, genuine aluminosilicate particles (no. 29 and no. 32; Fig. S10) and Fe-rich particles (no. 2 and no. 7; Fig. S11) did not show hygroscopic growth with changing RH.

4 Atmospheric implications

The investigation of the hygroscopic behavior of ambient SSAs is crucial for understanding the atmospheric chemistry and physics of marine environments. Previous studies have recognized that SSAs contain a wide range of inorganic sea salt and organic species (Schiffer et al., 2018), making it difficult to assess their hygroscopicity. In this study, the hygroscopic behavior of SSAs was systematically characterized and correlated with the role of inorganic salt moieties and enriched organic material coating. It was found that SSAs partially dissolve at lower RHs than the inorganic surrogates, including (Na, Mg)(Cl, NO_3), due to the coexistence with other soluble moieties such as water-soluble secondary organics. This indicates that SSAs will be increasingly susceptible to trace gas species and subsequent heterogeneous chemical reactions (Lee et al., 2020). The degree of chloride depletion was also found to affect the hygroscopic behavior of aged SSAs. SSAs with a higher degree of chloride depletion, i.e., higher aging degree, tend to exhibit multiple phase transitions with reducing RH, thus retaining the phase-separated core shell mixing state, which impacts aerosol–radiation interactions (Sun et al., 2018). The importance of considering these surrogate systems when modeling the hygroscopic behavior of ambient SSAs is apparent, especially in the case of field observations, where a wide range of mixing states exist in particles. Even though there are still discrepancies

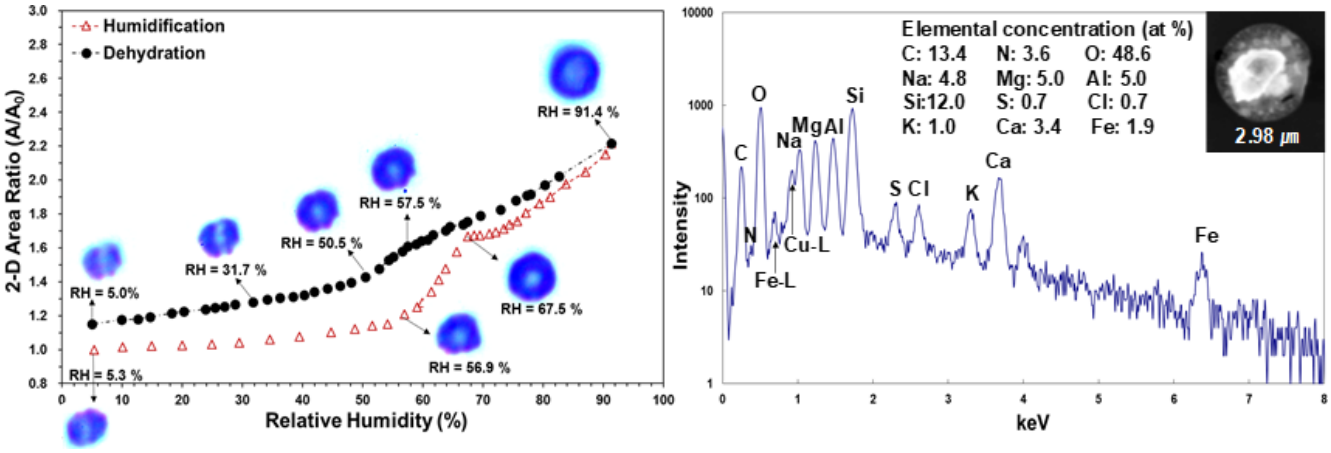

Figure 8. 2-D area ratio plot, X-ray spectrum, and SEM image with diameter of an aged aluminosilicate particle mixed with SSA (particle no. 14).

regarding whether the organic fraction can influence the hygroscopic growth of SSAs, this study demonstrated that organic substances covering the sea salt moieties did suppress their hygroscopic growth. Further investigations, including obtaining exact elemental and molecular compositions of the organic shells, are needed to examine the aging of SSAs and quantify their uncertain effects on SSAs' hygroscopicity in thermodynamic models.

In addition, other species involving mineral dust and anthropogenic particles can be transported into marine environments and mixed with SSAs, which alter the particle compositions and, in turn, their hygroscopicity. Heterogeneous mixing or coating of SSAs onto less hygroscopic dust particles can enhance their ability to interact with water vapor and reactive trace gases, leading to the formation of new particles and increased cloud condensation nuclei (CCN) activity (Tang et al., 2016). This mixing can also affect the optical properties and radiative forcing of atmospheric aerosols, as the scattering and absorption of solar radiation by aerosols are dependent on their size, composition, and mixing state. Furthermore, the impact of anthropogenic emissions on the hygroscopicity of marine aerosols is an important area of research, as increased levels of atmospheric pollutants may enhance the aerosol–water interaction and lead to changes in cloud properties and precipitation patterns (Su et al., 2022). Therefore, a comprehensive understanding of the hygroscopic behavior of marine aerosols and their interactions with other atmospheric constituents is necessary for accurately predicting their impacts on climate and air quality.

5 Conclusions

The hygroscopic behavior of individual ambient aerosol particles collected at a coastal site of Jeju Island, South Korea, was investigated in correlation with their chemical compositions derived from X-ray microanalysis. Specifically, we focused on the hygroscopic behavior of ambient aged SSAs and their dependence on the extent of reaction between Cl^- and NO_3^- ions, estimated from the mixing ratios of these ions using SEM-EDX. The phase transitions of the aged SSAs were found to be dominated by inorganics involving Na(Cl, NO_3) and/or (Na, Mg)(Cl, NO_3) systems, with organic surfactant films covering the droplets and suppressing hygroscopic growth and shrinkage with changing RH. For Cl-rich SSAs, two major transitions were observed during the humidification process. The first was at the MDRH and the second at a final DRH. During the dehydration process, Cl-rich SSAs showed single-stage efflorescence. Cl-depleted SSAs showed two prompt deliquescence transitions during the humidification process and stepwise transitions during the dehydration process, depending on their chemical compositions.

The hygroscopic behavior of other particle types, including aged aluminosilicate, Ca-containing, organic and ammonium sulfate mixture, and Fe-rich particles, was also observed. Aged mineral particles showed varying degrees of size changes with changing RH, potentially due to the presence of SSAs and/or NO_3^- species resulting from coagulation and heterogeneous reactions, while non-reacted mineral and Fe-rich particles did not exhibit significant size changes during the hygroscopic process. The mixture particles of organic and ammonium sulfate displayed lower DRH and ERH values compared to pure ammonium sulfate salt, indicating the impact of organic species on the hygroscopic behavior of ammonium sulfate. While there have been some studies on the hygroscopic behavior of ambient marine aerosols, this study is one of the first to systematically investigate their hygroscopic behavior and to correlate it with their chemical compositions, thus providing better insights into their impact on climate change and atmospheric chemistry.

Data availability. The data used in this study are available upon request; please contact Chul-Un Ro (curo@inha.ac.kr).

Supplement. The supplement related to this article is available online at: https://doi.org/10.5194/acp-23-12571-2023-supplement.

Author contributions. LW, HJE, HY, DG, and HRC designed the experiment. LW, HJE, HY, and HRC carried out the measurements and/or analyzed the data. LW, HJE, HY, DG, HRC, PF, and CUR contributed discussion of the data. LW, HJE, DG, and CUR drafted the paper.

Competing interests. The contact author has declared that none of the authors has any competing interests.

Disclaimer. Publisher's note: Copernicus Publications remains neutral with regard to jurisdictional claims made in the text, published maps, institutional affiliations, or any other geographical representation in this paper. While Copernicus Publications makes every effort to include appropriate place names, the final responsibility lies with the authors.

Acknowledgements. This study has been supported by the National Research Foundation of Korea (NRF) grant funded by the South Korean government (MSIT; grant nos. 2021R1A4A1032579 and 2021R1A2C2004240) and by the National Institute of Environmental Research (NIER) funded by the Ministry of Environment (MOE) of South Korea (grant no. NIER-2021-03-03-007).

Financial support. This research has been supported by the National Research Foundation of Korea (NRF) grant funded by the South Korean government (MSIT; grant nos. 2021R1A4A1032579 and 2021R1A2C2004240) and by the National Institute of Environmental Research (NIER) funded by the Ministry of Environment (MOE) of South Korea (grant no. NIER-2021-03-03-007).

Review statement. This paper was edited by Markus Ammann and reviewed by two anonymous referees.

References

Ahn, K.-H., Kim, S.-M., Jung, H.-J., Lee, M.-J., Eom, H.-J., Maskey, S., and Ro, C.-U.: Combined Use of Optical and Electron Microscopic Techniques for the Measurement of Hygroscopic Property, Chemical Composition, and Morphology of Individual Aerosol Particles, Anal. Chem., 82, 7999–8009, https://doi.org/10.1021/ac101432y, 2010.

Ansari, A. S. and Pandis, S. N.: Prediction of multicomponent inorganic atmospheric aerosol behavior, Atmos. Environ., 33, 745–757, https://doi.org/10.1016/S1352-2310(98)00221-0, 1999.

Atkinson, D. B., Radney, J. G., Lum, J., Kolesar, K. R., Cziczo, D. J., Pekour, M. S., Zhang, Q., Setyan, A., Zelenyuk, A., and Cappa, C. D.: Aerosol optical hygroscopicity measurements during the 2010 CARES campaign, Atmos. Chem. Phys., 15, 4045–4061, https://doi.org/10.5194/acp-15-4045-2015, 2015.

Ault, A. P., Moffet, R. C., Baltrusaitis, J., Collins, D. B., Ruppel, M. J., Cuadra-Rodriguez, L. A., Zhao, D., Guasco, T. L., Ebben, C. J., Geiger, F. M., Bertram, T. H., Prather, K. A., and Grassian, V. H.: Size-Dependent Changes in Sea Spray Aerosol Composition and Properties with Different Seawater Conditions, Environ. Sci. Technol., 47, 5603–5612, https://doi.org/10.1021/es400416g, 2013.

Ault, A. P., Guasco, T. L., Baltrusaitis, J., Ryder, O. S., Trueblood, J. V., Collins, D. B., Ruppel, M. J., Cuadra-Rodriguez, L. A., Prather, K. A., and Grassian, V. H.: Heterogeneous Reactivity of Nitric Acid with Nascent Sea Spray Aerosol: Large Differences Observed between and within Individual Particles, J. Phys. Chem. Lett., 5, 2493–2500, https://doi.org/10.1021/jz5008802, 2014.

Beardsley, R., Jang, M., Ori, B., Im, Y., Delcomyn, C. A., and Witherspoon, N.: Role of sea salt aerosols in the formation of aromatic secondary organic aerosol: yields and hygroscopic properties, Environ. Chem., 10, 167–177, https://doi.org/10.1071/EN13016, 2013.

Bertram, T. H., Cochran, R. E., Grassian, V. H., and Stone, E. A.: Sea spray aerosol chemical composition: elemental and molecular mimics for laboratory studies of heterogeneous and multiphase reactions, Chem. Soc. Rev., 47, 2374–2400, https://doi.org/10.1039/c7cs00008a, 2018.

Carslaw, K. S., Clegg, S. L., and Brimblecombe, P.: A Thermodynamic Model of the System HCl-HNO3-H2SO4-H2O, Including Solubilities of HBr, from $<$ 200 to 328 K, J. Phys. Chem. A, 99, 11557–11574, https://doi.org/10.1021/j100029a039, 1995.

Chan, C. K., Liang, Z., Zheng, J., Clegg, S. L., and Brimblecombe, P.: Thermodynamic properties of aqueous aerosols to high supersaturation: I – measurements of water activity of the system Na^+–Cl^-–NO_3^-–SO_4^{2-}–H_2O at $\sim$ 298.15 K, Aerosol Sci. Technol., 27, 324–344, https://doi.org/10.1080/02786829708965477, 1997.

Chan, C. K., Ha, Z., and Choi, M. Y.: Study of water activities of aerosols of mixtures of sodium and magnesium salts, Atmos. Environ., 34, 4795–4803, https://doi.org/10.1016/S1352-2310(00)00252-1, 2000.

Chang, S.-Y. and Lee, C.-T.: Applying GC-TCD to investigate the hygroscopic characteristics of mixed aerosols, Atmos. Environ., 36, 1521–1530, https://doi.org/10.1016/S1352-2310(01)00546-5, 2002.

Clegg, S. L., Brimblecombe, P., and Wexler, A. S.: Thermodynamic Model of the System H^+–NH_4^+–Na^+–SO_4^{2-}–NO_3^-–Cl^-–H_2O at 298.15 K, J. Phys. Chem. A, 102, 2155–2171, https://doi.org/10.1021/jp973043j, 1998a.

Clegg, S. L., Brimblecombe, P., and Wexler, A. S.: Thermodynamic Model of the System H^+–NH_4^+–SO_4^{2-}–NO_3^-–H_2O at Tropospheric Temperatures, J. Phys. Chem. A, 102, 2137–2154, https://doi.org/10.1021/jp973042r, 1998b.

Cochran, R. E., Laskina, O., Jayarathne, T., Laskin, A., Laskin, J., Lin, P., Sultana, C., Lee, C., Moore, K. A., Cappa, C. D., Bertram, T. H., Prather, K. A., Grassian, V. H., and Stone, E. A.: Analysis of Organic Anionic Surfac-

tants in Fine and Coarse Fractions of Freshly Emitted Sea Spray Aerosol, Environ. Sci. Technol., 50, 2477–2486, https://doi.org/10.1021/acs.est.5b04053, 2016.

Cochran, R. E., Laskina, O., Trueblood, J. V., Estillore, A. D., Morris, H. S., Jayarathne, T., Sultana, C. M., Lee, C., Lin, P., Laskin, J., Laskin, A., Dowling, J. A., Qin, Z., Cappa, C. D., Bertram, T. H., Tivanski, A. V., Stone, E. A., Prather, K. A., and Grassian, V. H.: Molecular Diversity of Sea Spray Aerosol Particles: Impact of Ocean Biology on Particle Composition and Hygroscopicity, Chem, 2, 655–667, https://doi.org/10.1016/j.chempr.2017.03.007, 2017.

Cohen, M. D., Flagan, R. C., and Seinfeld, J. H.: Studies of concentrated electrolyte solutions using the electrodynamic balance. 3. Solute nucleation, J. Phys. Chem., 91, 4583–4590, https://doi.org/10.1021/j100301a031, 1987.

Cziczo, D. J., Nowak, J. B., Hu, J. H., and Abbatt, J. P. D.: Infrared spectroscopy of model tropospheric aerosols as a function of relative humidity: Observation of deliquescence and crystallization, J. Geophys. Res.-Atmos., 102, 18843–18850, https://doi.org/10.1029/97jd01361, 1997.

Eom, H.-J., Gupta, D., Li, X., Jung, H.-J., Kim, H., and Ro, C.-U.: Influence of Collecting Substrates on the Characterization of Hygroscopic Properties of Inorganic Aerosol Particles, Anal. Chem., 86, 2648–2656, https://doi.org/10.1021/ac4042075, 2014.

Eom, H.-J., Gupta, D., Cho, H.-R., Hwang, H. J., Hur, S. D., Gim, Y., and Ro, C.-U.: Single-particle investigation of summertime and wintertime Antarctic sea spray aerosols using low-Z particle EPMA, Raman microspectrometry, and ATR-FTIR imaging techniques, Atmos. Chem. Phys., 16, 13823–13836, https://doi.org/10.5194/acp-16-13823-2016, 2016.

Finlayson-Pitts, B. J. and Pitts, J. N.: Chemistry of the upper and lower atmosphere: theory, experiments, and applications, Academic Press, San Diego, ISBN: 978-0-12-257060-5, 2000.

Forestieri, S. D., Cornwell, G. C., Helgestad, T. M., Moore, K. A., Lee, C., Novak, G. A., Sultana, C. M., Wang, X., Bertram, T. H., Prather, K. A., and Cappa, C. D.: Linking variations in sea spray aerosol particle hygroscopicity to composition during two microcosm experiments, Atmos. Chem. Phys., 16, 9003–9018, https://doi.org/10.5194/acp-16-9003-2016, 2016.

Freney, E. J., Adachi, K., and Buseck, P. R.: Internally mixed atmospheric aerosol particles: Hygroscopic growth and light scattering, J. Geophys. Res.-Atmos., 115, D19210, https://doi.org/10.1029/2009jd013558, 2010.

Gard, E. E., Kleeman, M. J., Gross, D. S., Hughes, L. S., Allen, J. O., Morrical, B. D., Fergenson, D. P., Dienes, T., Ga¨lli, M. E., and Johnson, R. J.: Direct observation of heterogeneous chemistry in the atmosphere, Science, 279, 1184–1187, https://doi.org/10.1126/science.279.5354.1184, 1998.

Ge, Z., Wexler, A. S., and Johnston, M. V.: Multicomponent Aerosol Crystallization, J. Colloid Interf. Sci., 183, 68–77, https://doi.org/10.1006/jcis.1996.0519, 1996.

Ge, Z., Wexler, A. S., and Johnston, M. V.: Deliquescence Behavior of Multicomponent Aerosols, J. Phys. Chem. A, 102, 173–180, https://doi.org/10.1021/jp972396f, 1998.

Geng, H., Kang, S., Jung, H. J., Choël, M., Kim, H., and Ro, C. U.: Characterization of individual submicrometer aerosol particles collected in Incheon, Korea, by quantitative transmission electron microscopy energy-dispersive X-ray spectrometry, J. Geophys. Res.-Atmos., 115, D15306, https://doi.org/10.1029/2009JD013486, 2010.

Geng, H., Hwang, H., Liu, X., Dong, S., and Ro, C.-U.: Investigation of aged aerosols in size-resolved Asian dust storm particles transported from Beijing, China, to Incheon, Korea, using low-Z particle EPMA, Atmos. Chem. Phys., 14, 3307–3323, https://doi.org/10.5194/acp-14-3307-2014, 2014.

Ghorai, S., Wang, B., Tivanski, A., and Laskin, A.: Hygroscopic properties of internally mixed particles composed of NaCl and water-soluble organic acids, Environ. Sci. Technol., 48, 2234–2241, https://doi.org/10.1021/es404727u, 2014.

Guo, L., Gu, W., Peng, C., Wang, W., Li, Y. J., Zong, T., Tang, Y., Wu, Z., Lin, Q., Ge, M., Zhang, G., Hu, M., Bi, X., Wang, X., and Tang, M.: A comprehensive study of hygroscopic properties of calcium- and magnesium-containing salts: implication for hygroscopicity of mineral dust and sea salt aerosols, Atmos. Chem. Phys., 19, 2115–2133, https://doi.org/10.5194/acp-19-2115-2019, 2019.

Gupta, D., Eom, H.-J., Cho, H.-R., and Ro, C.-U.: Hygroscopic behavior of NaCl–$MgCl_2$ mixture particles as nascent sea-spray aerosol surrogates and observation of efflorescence during humidification, Atmos. Chem. Phys., 15, 11273–11290, https://doi.org/10.5194/acp-15-11273-2015, 2015a.

Gupta, D., Kim, H., Park, G., Li, X., Eom, H.-J., and Ro, C.-U.: Hygroscopic properties of NaCl and $NaNO_3$ mixture particles as reacted inorganic sea-salt aerosol surrogates, Atmos. Chem. Phys., 15, 3379–3393, https://doi.org/10.5194/acp-15-3379-2015, 2015b.

Haynes, W. M.: CRC Handbook of Chemistry and Physics, 96th edn., CRC Press, Boca Raton, Florida, 14–18, ISBN: 978-1482260960, 2015.

Haywood, J. and Boucher, O.: Estimates of the direct and indirect radiative forcing due to tropospheric aerosols: A review, Rev. Geophys., 38, 513–543, https://doi.org/10.1029/1999rg000078, 2000.

Herich, H., Kammermann, L., Friedman, B., Gross, D. S., Weingartner, E., Lohmann, U., Spichtinger, P., Gysel, M., Baltensperger, U., and Cziczo, D. J.: Subarctic atmospheric aerosol composition: 2. Hygroscopic growth properties, J. Geophys. Res.-Atmos., 114, D13204, https://doi.org/10.1029/2008jd011574, 2009.

Keene, W. C., Maring, H., Maben, J. R., Kieber, D. J., Pszenny, A. A. P., Dahl, E. E., Izaguirre, M. A., Davis, A. J., Long, M. S., Zhou, X., Smoydzin, L., and Sander, R.: Chemical and physical characteristics of nascent aerosols produced by bursting bubbles at a model air-sea interface, J. Geophys. Res.-Atmos., 112, D21202, https://doi.org/10.1029/2007jd008464, 2007.

Kim, H., Lee, M.-J., Jung, H.-J., Eom, H.-J., Maskey, S., Ahn, K.-H., and Ro, C.-U.: Hygroscopic behavior of wet dispersed and dry deposited $NaNO_3$ particles, Atmos. Environ., 60, 68–75, https://doi.org/10.1016/j.atmosenv.2012.06.011, 2012.

Kong, X., Wolf, M. J., Roesch, M., Thomson, E. S., Bartels-Rausch, T., Alpert, P. A., Ammann, M., Prisle, N. L., and Cziczo, D. J.: A continuous flow diffusion chamber study of sea salt particles acting as cloud nuclei: deliquescence and ice nucleation, Tellus B, 70, 1–11, https://doi.org/10.1080/16000889.2018.1463806, 2018.

Krieger, U. K., Marcolli, C., and Reid, J. P.: Exploring the complexity of aerosol particle properties and processes using

single particle techniques, Chem. Soc. Rev., 41, 6631–6662, https://doi.org/10.1039/c2cs35082c, 2012.

Krueger, B. J., Grassian, V. H., Iedema, M. J., Cowin, J. P., and Laskin, A.: Probing Heterogeneous Chemistry of Individual Atmospheric Particles Using Scanning Electron Microscopy and Energy-Dispersive X-ray Analysis, Anal. Chem., 75, 5170–5179, https://doi.org/10.1021/ac034455t, 2003.

Laskin, A., Moffet, R. C., Gilles, M. K., Fast, J. D., Zaveri, R. A., Wang, B., Nigge, P., and Shutthanandan, J.: Tropospheric chemistry of internally mixed sea salt and organic particles: Surprising reactivity of NaCl with weak organic acids, J. Geophys. Res., 117, D15302, https://doi.org/10.1029/2012JD017743, 2012.

Lee, H. D., Morris, H. S., Laskina, O., Sultana, C. M., Lee, C., Jayarathne, T., Cox, J. L., Wang, X., Hasenecz, E. S., DeMott, P. J., Bertram, T. H., Cappa, C. D., Stone, E. A., Prather, K. A., Grassian, V. H., and Tivanski, A. V.: Organic Enrichment, Physical Phase State, and Surface Tension Depression of Nascent Core–Shell Sea Spray Aerosols during Two Phytoplankton Blooms, ACS Earth Space Chem., 4, 650–660, https://doi.org/10.1021/acsearthspacechem.0c00032, 2020.

Li, X., Gupta, D., Eom, H.-J., Kim, H., and Ro, C.-U.: Deliquescence and efflorescence behavior of individual NaCl and KCl mixture aerosol particles, Atmos. Environ., 82, 36–43, https://doi.org/10.1016/j.atmosenv.2013.10.011, 2014.

Li, X., Wu, L., Lee, J.-S., and Ro, C.-U.: Hygroscopic behavior and chemical reactivity of aerosols generated from mixture solutions of low molecular weight dicarboxylic acids and NaCl, Phys. Chem. Chem. Phys., 23, 11052–11064, https://doi.org/10.1039/d1cp00590a, 2021.

Li, Y. J., Liu, P. F., Bergoend, C., Bateman, A. P., and Martin, S. T.: Rebounding hygroscopic inorganic aerosol particles: Liquids, gels, and hydrates, Aerosol Sci. Technol., 51, 388–396, https://doi.org/10.1080/02786826.2016.1263384, 2016.

Liu, Y. and Laskin, A.: Hygroscopic Properties of CH_3SO_3Na, $CH_3SO_3NH_4$, $(CH_3SO_3)_2Mg$, and $(CH_3SO_3)_2Ca$ Particles Studied by micro-FTIR Spectroscopy, J. Phys. Chem. A, 113, 1531–1538, https://doi.org/10.1021/jp8079149, 2009.

Liu, Y., Cain, J. P., Wang, H., and Laskin, A.: Kinetic Study of Heterogeneous Reaction of Deliquesced NaCl Particles with Gaseous HNO_3 Using Particle-on-Substrate Stagnation Flow Reactor Approach, J. Phys. Chem. A, 111, 10026–10043, https://doi.org/10.1021/jp072005p, 2007.

Liu, Y., Minofar, B., Desyaterik, Y., Dames, E., Zhu, Z., Cain, J. P., Hopkins, R. J., Gilles, M. K., Wang, H., and Jungwirth, P.: Internal structure, hygroscopic and reactive properties of mixed sodium methanesulfonate-sodium chloride particles, Phys. Chem. Chem. Phys., 13, 11846–11857, https://doi.org/10.1039/C1CP20444K, 2011.

Martin, S. T.: Phase Transitions of Aqueous Atmospheric Particles, Chem. Rev., 100, 3403–3454, https://doi.org/10.1021/cr990034t, 2000.

Meskhidze, N., Petters, M. D., Tsigaridis, K., Bates, T., O'Dowd, C., Reid, J., Lewis, E. R., Gantt, B., Anguelova, M. D., Bhave, P. V., Bird, J., Callaghan, A. H., Ceburnis, D., Chang, R., Clarke, A., de Leeuw, G., Deane, G., DeMott, P. J., Elliot, S., Facchini, M. C., Fairall, C. W., Hawkins, L., Hu, Y., Hudson, J. G., Johnson, M. S., Kaku, K. C., Keene, W. C., Kieber, D. J., Long, M. S., Mårtensson, M., Modini, R. L., Osburn, C. L., Prather, K. A., Pszenny, A., Rinaldi, M., Russell, L. M., Salter, M., Sayer, A. M., Smirnov, A., Suda, S. R., Toth, T. D., Worsnop, D. R., Wozniak, A., and Zorn, S. R.: Production mechanisms, number concentration, size distribution, chemical composition, and optical properties of sea spray aerosols, Atmos. Sci. Lett., 14, 207–213, https://doi.org/10.1002/asl2.441, 2013.

Mikhailov, E., Vlasenko, S., Martin, S. T., Koop, T., and Pöschl, U.: Amorphous and crystalline aerosol particles interacting with water vapor: conceptual framework and experimental evidence for restructuring, phase transitions and kinetic limitations, Atmos. Chem. Phys., 9, 9491–9522, https://doi.org/10.5194/acp-9-9491-2009, 2009.

Ming, Y. and Russell, L. M.: Predicted hygroscopic growth of sea salt aerosol, J. Geophys. Res.-Atmos., 106, 28259–28274, https://doi.org/10.1029/2001jd000454, 2001.

Nguyen, Q. T., Kjær, K. H., Kling, K. I., Boesen, T., and Bilde, M.: Impact of fatty acid coating on the CCN activity of sea salt particles, Tellus B, 69, 1304064, https://doi.org/10.1080/16000889.2017.1304064, 2017.

Niedermeier, D., Wex, H., Voigtländer, J., Stratmann, F., Brüggemann, E., Kiselev, A., Henk, H., and Heintzenberg, J.: LACIS-measurements and parameterization of sea-salt particle hygroscopic growth and activation, Atmos. Chem. Phys., 8, 579–590, https://doi.org/10.5194/acp-8-579-2008, 2008.

O'Dowd, C. D. and de Leeuw, G.: Marine aerosol production: a review of the current knowledge, Philos. T. Roy. Soc. A, 365, 1753–1774, https://doi.org/10.1098/rsta.2007.2043, 2007.

Pandis, S. N., Wexler, A. S., and Seinfeld, J. H.: Dynamics of Tropospheric Aerosols, J. Phys. Chem., 99, 9646–9659, https://doi.org/10.1021/j100024a003, 1995.

Pöschl, U. and Shiraiwa, M.: Multiphase Chemistry at the Atmosphere–Biosphere Interface Influencing Climate and Public Health in the Anthropocene, Chem. Rev., 115, 4440–4475, https://doi.org/10.1021/cr500487s, 2015.

Pósfai, M., Anderson, J. R., Buseck, P. R., and Sievering, H.: Compositional variations of sea-salt-mode aerosol particles from the North Atlantic, J. Geophys. Res.-Atmos., 100, 23063–23074, https://doi.org/10.1029/95jd01636, 1995.

Prather, K. A., Bertram, T. H., Grassian, V. H., Deane, G. B., Stokes, M. D., DeMott, P. J., Aluwihare, L. I., Palenik, B. P., Azam, F., Seinfeld, J. H., Moffet, R. C., Molina, M. J., Cappa, C. D., Geiger, F. M., Roberts, G. C., Russell, L. M., Ault, A. P., Baltrusaitis, J., Collins, D. B., Corrigan, C. E., Cuadra-Rodriguez, L. A., Ebben, C. J., Forestieri, S. D., Guasco, T. L., Hersey, S. P., Kim, M. J., Lambert, W. F., Modini, R. L., Mui, W., Pedler, B. E., Ruppel, M. J., Ryder, O. S., Schoepp, N. G., Sullivan, R. C., and Zhao, D.: Bringing the ocean into the laboratory to probe the chemical complexity of sea spray aerosol, P. Natl. Acad. Sci. USA, 110, 7550–7555, https://doi.org/10.1073/pnas.1300262110, 2013.

Quinn, P. K., Collins, D. B., Grassian, V. H., Prather, K. A., and Bates, T. S.: Chemistry and Related Properties of Freshly Emitted Sea Spray Aerosol, Chem. Rev., 115, 4383–4399, https://doi.org/10.1021/cr500713g, 2015.

Rosati, B., Christiansen, S., Dinesen, A., Roldin, P., Massling, A., Nilsson, E. D., and Bilde, M.: The impact of atmospheric oxidation on hygroscopicity and cloud droplet activation of inorganic sea spray aerosol, Sci. Rep.-UK, 11, 10008, https://doi.org/10.1038/s41598-021-89346-6, 2021.

Ryder, O. S., Ault, A. P., Cahill, J. F., Guasco, T. L., Riedel, T. P., Cuadra-Rodriguez, L. A., Gaston, C. J., Fitzgerald, E., Lee, C., Prather, K. A., and Bertram, T. H.: On the Role of Particle Inorganic Mixing State in the Reactive Uptake of N_2O_5 to Ambient Aerosol Particles, Environ. Sci. Technol., 48, 1618–1627, https://doi.org/10.1021/es4042622, 2014.

Saul, T. D., Tolocka, M. P., and Johnston, M. V.: Reactive Uptake of Nitric Acid onto Sodium Chloride Aerosols Across a Wide Range of Relative Humidities, J. Phys. Chem. A, 110, 7614–7620, https://doi.org/10.1021/jp060639a, 2006.

Schiffer, J. M., Mael, L. E., Prather, K. A., Amaro, R. E., and Grassian, V. H.: Sea Spray Aerosol: Where Marine Biology Meets Atmospheric Chemistry, ACS Central Science, 4, 1617–1623, https://doi.org/10.1021/acscentsci.8b00674, 2018.

Schill, S. R., Collins, D. B., Lee, C., Morris, H. S., Novak, G. A., Prather, K. A., Quinn, P. K., Sultana, C. M., Tivanski, A. V., Zimmermann, K., Cappa, C. D., and Bertram, T. H.: The Impact of Aerosol Particle Mixing State on the Hygroscopicity of Sea Spray Aerosol, ACS Central Science, 1, 132–141, https://doi.org/10.1021/acscentsci.5b00174, 2015.

Schindelholz, E., Risteen, B., and Kelly, R.: Effect of relative humidity on corrosion of steel under sea salt aerosol proxies: I. NaCl, J. Electrochem. Soc., 161, C450, https://doi.org/10.1149/2.0221410jes, 2014.

Seinfeld, J. H. and Pandis, S. N.: Atmospheric chemistry and physics: from air pollution to climate change, 2nd edn., J. Wiley, Hoboken, NJ, 1203 pp., ISBN: 978-0471720188, 2006.

Semeniuk, T. A., Wise, M. E., Martin, S. T., Russell, L. M., and Buseck, P. R.: Water uptake characteristics of individual atmospheric particles having coatings, Atmos. Environ., 41, 6225–6235, https://doi.org/10.1016/j.atmosenv.2007.04.001, 2007.

Song, Y., Li, J., Tsona, N. T., Liu, L., and Du, L.: Enrichment of short-chain organic acids transferred to submicron sea spray aerosols, Sci. Total Environ., 851, 158122, https://doi.org/10.1016/j.scitotenv.2022.158122, 2022.

Su, B., Wang, T., Zhang, G., Liang, Y., Lv, C., Hu, Y., Li, L., Zhou, Z., Wang, X., and Bi, X.: A review of atmospheric aging of sea spray aerosols: Potential factors affecting chloride depletion, Atmos. Environ., 290, 119365, https://doi.org/10.1016/j.atmosenv.2022.119365, 2022.

Sun, J., Liu, L., Xu, L., Wang, Y., Wu, Z., Hu, M., Shi, Z., Li, Y., Zhang, X., Chen, J., and Li W.,: Key role of nitrate in phase transitions of urban particles: implications of important reactive surfaces for secondary aerosol formation, J. Geophys. Res.-Atmos., 123, 1234–1243, https://doi.org/10.1002/2017JD027264, 2018.

Tang, I. N., Tridico, A. C., and Fung, K. H.: Thermodynamic and optical properties of sea salt aerosols, J. Geophys. Res.-Atmos., 102, 23269–23275, https://doi.org/10.1029/97jd01806, 1997.

Tang, M., Cziczo, D. J., and Grassian, V. H.: Interactions of water with mineral dust aerosol: water adsorption, hygroscopicity, cloud condensation, and ice nucleation, Chem. Rev., 116, 4205–4259, https://doi.org/10.1021/acs.chemrev.5b00529, 2016.

ten Brink, H. M.: Reactive uptake of HNO_3 and H_2SO_4 in sea-salt (NaCl) particles, J. Aerosol Sci., 29, 57–64, https://doi.org/10.1016/S0021-8502(97)00460-6, 1998.

Tobon, Y. A., El Hajj, D., Seng, S., Bengrad, F., Moreau, M., Visez, N., Chiapello, I., Crumeyrolle, S., and Choel, M.: Impact of the particle mixing state on the hygroscopicity of internally mixed sodium chloride-ammonium sulfate single droplets: a theoretical and experimental study, Phys. Chem. Chem. Phys., 23, 14391–14403, https://doi.org/10.1039/d1cp01574e, 2021.

Vaishya, A., Ovadnevaite, J., Bialek, J., Jennings, S. G., Ceburnis, D., and O'Dowd, C. D.: Bistable effect of organic enrichment on sea spray radiative properties, Geophys. Res. Lett., 40, 6395–6398, https://doi.org/10.1002/2013gl058452, 2013.

Vekemans, B., Janssens, K., Vincze, L., Adams, F., and Van Espen, P.: Analysis of X-ray spectra by iterative least squares (AXIL): New developments, X-Ray Spectrom., 23, 278–285, https://doi.org/10.1002/xrs.1300230609, 1994.

Wang, J. and Martin, S. T.: Satellite characterization of urban aerosols: Importance of including hygroscopicity and mixing state in the retrieval algorithms, J. Geophys. Res.-Atmos., 112, D17203, https://doi.org/10.1029/2006jd008078, 2007.

Wang, X., Sultana, C. M., Trueblood, J., Hill, T. C., Malfatti, F., Lee, C., Laskina, O., Moore, K. A., Beall, C. M., and McCluskey, C. S.: Microbial control of sea spray aerosol composition: A tale of two blooms, ACS Central Science, 1, 124–131, https://doi.org/10.1021/acscentsci.5b00148, 2015.

Wang, X., Deane, G. B., Moore, K. A., Ryder, O. S., Stokes, M. D., Beall, C. M., Collins, D. B., Santander, M. V., Burrows, S. M., Sultana, C. M., and Prather, K. A.: The role of jet and film drops in controlling the mixing state of submicron sea spray aerosol particles, P. Natl. Acad. Sci. USA, 114, 6978–6983, https://doi.org/10.1073/pnas.1702420114, 2017.

Wexler, A. S. and Clegg, S. L.: Atmospheric aerosol models for systems including the ions H^+, NH_4^+, Na^+, SO_4^{2-}, NO_3^-, Cl^-, Br^-, and H_2O, J. Geophys. Res., 107, 4207, https://doi.org/10.1029/2001jd000451, 2002.

Wexler, A. S. and Seinfeld, J. H.: Second-generation inorganic aerosol model, Atmos. Environ. A-Gen., 27, 2731–2748, https://doi.org/10.1016/0960-1686(91)90203-J, 1991.

Wise, M. E., Semeniuk, T. A., Bruintjes, R., Martin, S. T., Russell, L. M., and Buseck, P. R.: Hygroscopic behavior of NaCl-bearing natural aerosol particles using environmental transmission electron microscopy, J. Geophys. Res.-Atmos., 112, D10224, https://doi.org/10.1029/2006jd007678, 2007.

Wise, M. E., Freney, E. J., Tyree, C. A., Allen, J. O., Martin, S. T., Russell, L. M., and Buseck, P. R.: Hygroscopic behavior and liquid-layer composition of aerosol particles generated from natural and artificial seawater, J. Geophys. Res.-Atmos., 114, D03201, https://doi.org/10.1029/2008jd010449, 2009.

Woods, E., Chung, D., Lanney, H. M., and Ashwell, B. A.: Surface Morphology and Phase Transitions in Mixed $NaCl/MgSO_4$ Aerosol Particles, J. Phys. Chem. A, 114, 2837–2844, https://doi.org/10.1021/jp911133j, 2010.

Woods, E., Heylman, K. D., Gibson, A. K., Ashwell, A. P., and Rossi, S. R.: Effects of NOy Aging on the Dehydration Dynamics of Model Sea Spray Aerosol, J. Phys. Chem. A, 117, 4214–4222, https://doi.org/10.1021/jp401646d, 2013.

Wu, L., Li, X., and Ro, C.-U.: Hygroscopic Behavior of Ammonium Sulfate, Ammonium Nitrate, and their Mixture Particles, Asian J. Atmos., 13, 196–211, https://doi.org/10.5572/ajae.2019.13.3.196, 2019.

Wu, L., Becote, C., Sobanska, S., Flaud, P.-M., Perraudin, E., Villenave, E., Song, Y.-C., and Ro, C.-U.: Hygroscopic behavior of aerosols generated from solutions of 3-methyl-1,2,3-butanetricarboxylic acid, its sodium salts, and its mix-

tures with NaCl, Atmos. Chem. Phys., 20, 14103–14122, https://doi.org/10.5194/acp-20-14103-2020, 2020.

Xiao, H.-S., Dong, J.-L., Wang, L.-Y., Zhao, L.-J., Wang, F., and Zhang, Y.-H.: Spatially resolved micro-raman observation on the phase separation of effloresced sea salt droplets, Environ. Sci. Technol., 42, 8698–8702, https://doi.org/10.1021/es801181f, 2008.

Xu, W., Ovadnevaite, J., Fossum, K. N., Lin, C., Huang, R.-J., O'Dowd, C., and Ceburnis, D.: Aerosol hygroscopicity and its link to chemical composition in the coastal atmosphere of Mace Head: marine and continental air masses, Atmos. Chem. Phys., 20, 3777–3791, https://doi.org/10.5194/acp-20-3777-2020, 2020.

Zhang, X., Massoli, P., Quinn, P. K., Bates, T. S., and Cappa, C. D.: Hygroscopic growth of submicron and supermicron aerosols in the marine boundary layer, J. Geophys. Res.-Atmos., 119, 8384–8399, https://doi.org/10.1002/2013jd021213, 2014.

Zhang, Y.-H., Choi, M. Y., and Chan, C. K.: Relating Hygroscopic Properties of Magnesium Nitrate to the Formation of Contact Ion Pairs, J. Phys. Chem. A, 108, 1712–1718, https://doi.org/10.1021/jp036524d, 2004.

Zhao, L.-J., Zhang, Y.-H., Wei, Z.-F., Cheng, H., and Li, X.-H.: Magnesium Sulfate Aerosols Studied by FTIR Spectroscopy: Hygroscopic Properties, Supersaturated Structures, and Implications for Seawater Aerosols, J. Phys. Chem. A, 110, 951–958, https://doi.org/10.1021/jp055291i, 2006.

Zieger, P., Vaisanen, O., Corbin, J. C., Partridge, D. G., Bastelberger, S., Mousavi-Fard, M., Rosati, B., Gysel, M., Krieger, U. K., Leck, C., Nenes, A., Riipinen, I., Virtanen, A., and Salter, M. E.: Revising the hygroscopicity of inorganic sea salt particles, Nat. Commun., 8, 15883, https://doi.org/10.1038/ncomms15883, 2017.

Zuend, A., Marcolli, C., Luo, B. P., and Peter, T.: A thermodynamic model of mixed organic-inorganic aerosols to predict activity coefficients, Atmos. Chem. Phys., 8, 4559–4593, https://doi.org/10.5194/acp-8-4559-2008, 2008.

Zuend, A., Marcolli, C., Booth, A. M., Lienhard, D. M., Soonsin, V., Krieger, U. K., Topping, D. O., McFiggans, G., Peter, T., and Seinfeld, J. H.: New and extended parameterization of the thermodynamic model AIOMFAC: calculation of activity coefficients for organic-inorganic mixtures containing carboxyl, hydroxyl, carbonyl, ether, ester, alkenyl, alkyl, and aromatic functional groups, Atmos. Chem. Phys., 11, 9155–9206, https://doi.org/10.5194/acp-11-9155-2011, 2011.